Journal of Computational Physics 435 (2021) 110215

Contents lists available at ScienceDirect

Journal of Computational Physics

www.elsevier.com/locate/jcp

Accurate and efficient approximations for generalized population balances incorporating coagulation and fragmentation

Mehakpreet Singh

Department of Chemical Sciences, Bernal Institute, University of Limerick, V94 T9PX Limerick, Ireland

ARTICLE INFO

Article history:
Available online 2 March 2021

Keywords:
Particles
Coagulation
Fragmentation
Nonlinear integro-partial differential equation
Finite volume scheme
Cell average technique

ABSTRACT

This study focuses on development of two approaches based on finite volume schemes for solving both one-dimensional and multidimensional nonlinear simultaneous coagulation-fragmentation population balance equations (PBEs). Existing finite volume schemes and sectional methods such as fixed pivot technique and cell average technique have many issues related to accuracy and efficiency. To resolve these challenges, two finite volume schemes are developed and compared with the cell average technique along with the exact solutions. The new schemes have features such as simpler mathematical formulations, easy to code and robust to apply on nonuniform grids. The numerical testing shows that both new finite volume schemes compute the number density functions and their corresponding integral moments with higher precision on a coarse grid by consuming lesser CPU time. In addition, both schemes are extended to approximate generalized simultaneous coagulation-fragmentation problems and retains the numerical accuracy and efficiency. For the higher dimensional PBEs (2D and 3D), the investigation and verification of the numerical schemes is done by deriving new exact integral moments for various combinations of coagulation kernels, selection functions and fragmentation kernels.

Contents

E-mail address: Mehakpreet.Singh@ul.ie.

https://doi.org/10.1016/j.jcp.2021.110215
0021-9991/

1. Introduction

Particulate processes tend to change particles properties such as size, mass, porosity and enthalpy due to various mechanisms such as coagulation, fragmentation, attrition, consolidation, nucleation and growth. A few of the important industrial scale applications (in chemical engineering and pharmaceutical sciences) involving these mechanisms are crystallization [35], depolymerization [1], high shear granulation [6], twin-screw granulation [14,21] and sprayed fluidized bed granulation [15]. However, in this paper, our primary emphasis is on the handling of a framework in which the properties of the particles are modified due to both coagulation and fragmentation processes. Coagulation (or Aggregation) is a mechanism in which two or more smaller particles come together to form a large size particle (see Fig. 1). During this process, the evolution of total number of particles decreases over time, while the mass remains conserved. In addition, as contrasted to coagulation, smaller particles are produced which increase the total number of particles in the system during the fragmentation mechanism, but the total mass remains unchanged. As a consequence of these mechanisms, various particles with different properties (size or volume) are produced in the system due to coagulation and fragmentation processes. In order to model such processes, mathematical models called *population balances* are needed to understand a change in the distribution of the particle property.

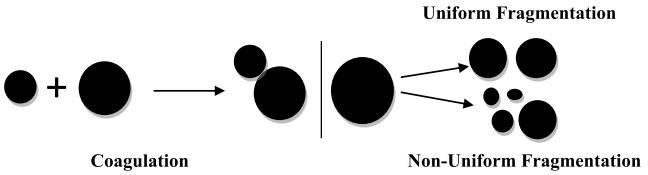

Fig. 1. Schematic diagram of coagulation and fragmentation processes.

Mathematically, the fragmentation and coagulation mechanisms can be classified as linear and nonlinear integro-partial differential equation, respectively. The one-dimensional simultaneous coagulation-fragmentation population balance model for a well mixed system which is used to describe the dynamics of the system [38] can be written as follows

$$\frac{\partial n(t,u)}{\partial t} = Q^{\pm}_{agg}(t,u) + Q^{\pm}_{brk}(t,u), \tag{1}$$

with initial condition $n(0,u) = n_0(u)$, $u \in \mathbb{R}_+$, where, $(t,u) \in \mathbb{R}^2_+$ and $\mathbb{R}_+ := (0,\infty)$. Further,

- $n(t,u)$: represents the number density function.
- $Q^{\pm}_{agg}(t,u)$: rate at which particles properties u are formed due to birth and death and is defined as

$$Q^{\pm}_{agg}(t,u) = \frac{1}{2}\int_0^u \beta(t,u-u',u')n(t,u-u')n(t,u')du' - \int_0^\infty \beta(t,u,u')n(t,u)n(t,u')du'. \tag{2}$$

In the above equation (2), the first term refers to the birth of the particle property u due to the merging of the particles properties $u-u'$ and u', whereas the second term corresponds to the death of the particle property u due to aggregation of the particle property u with any other particle. The coagulation kernel $\beta(t,u,u')$ describes the rate at which the particles properties u and u' forms a bigger size particle. Coagulation kernels are non-negative and symmetric with respect to volume arguments, that is, $\beta(t,u,u') = \beta(t,u',u)$. The conventional form of the coagulation kernel is $\beta(t,u,u') = \beta_0(t)\beta(u,u')$ and for simplicity we choose $\beta_0(t) = 1$.

- $Q^{\pm}_{brk}(t,u)$: rate at which the formation of the particles properties u takes place due to the fragmentation process and is defined by

$$Q^{\pm}_{brk}(t,u) = \int_{u}^{\infty} b(u,u')S(u')n(t,u')du' - S(u)n(t,u), \tag{3}$$

where the function $b(u,u')$ is the particle size distribution for the formation of particle property u from the particle property u'. Moreover, $S(u)$ is the selection function which describes the rate of selection of particle property u to break and mathematically can be written as $S(u) = S_0 s(u)$ where S_0 is considered to be 1 for the simple cases and $s(u) = 1,\ u$ and u^2. In addition, the function $b(u,u')$ must satisfy the following conditions:
(a) $\int_0^u b(u,u')du' = v(u)$, and
(b) $\int_0^{u'} ub(u,u')du' = u'$,
where $v(u)$ defines the number of fragments obtained from the fragmentation of particle property u and should be equal or bigger than 2.

To monitor the change in particles properties, the number density function $n(t,u)$ is essential to obtain, however, some integral properties such as moments are also of great interest [45,50,52] which is defined by

$$\mu_i(t) = \int_{0}^{\infty} u^i n(t,u)du, \tag{4}$$

for integers $i = 0, 1, 2, \ldots$. The zeroth moment ($\mu_0(t)$) represents the total number of particles and the first order moment ($\mu_1(t)$) defines total mass in the system.

Due to the presence of nonlinear integral in the equation (1), it is very challenging to find the exact solution for various coagulation kernels having complex structures such as Brownian kernel, kinetic theory of granular flow kernel along with Austin kernel corresponding to fragmentation equation. However, Patil and Andrews [32], Lin *et al.* [29] and Kaur *et al.* [16,17] were still able to derive the exact solutions for a simpler structured coagulation kernel (constant kernel) and binary fragmentation kernel ($b(u,u') = \frac{2}{u'}$) with linear selection rate ($S(u) = u$). Some other studies related to analytical solutions for higher dimensional population balance equations are provided by Fernández-Díaz and Gómez-García [10] and references therein. To overcome the issue of analytical solutions, many numerical methods including finite volume schemes [25,39,43,51], the method of moments [3,5,31,34], finite element method [2,8], Stochastic methods [13,30,33,56], Haar Wavelet [27] and sectional methods such as Fixed Pivot Technique [26,41,42] and Cell Average Technique [18,20,23,24,28,47] have been presented.

Among listed methods, the existing finite volume schemes [11,12,36] are well known for predicting the number density function accurately but do not focus on the accuracy of various order moments. Moreover, method of moments needs the conversion of original population balance equation into the moment form. Therefore, method of moments approaches merely focused on capturing the moments of different order accurately and lose the knowledge of the number density function. However, Monte Carlo methods are the most suitable numerical methods for approximating the coagulation-fragmentation mechanisms but a large number of particles are required in the system to approximate the number density function and various moments accurately which makes them computationally very expensive. This leads us to the choice of sectional methods whose ability to predict moments as well as number density function is excellent. But, the complex mathematical formulations of sectional methods are their major drawbacks which further restrict them to extend for solving higher dimensional population balance equations [7,46]. Attarakih *et al.* [4] developed a conservative discretization approach for approximating a one dimensional droplet breakage equation for interacting liquid-liquid dispersion which is highly accurate and efficient. For achieving the accuracy of the numerical results [4], 50 nonuniform cells were used and no extension in the higher dimensional equations is available in literature. Hence, unable to apply on the applications such as granulation [40] in which two or more particles properties are required to be tracked.

Recently, Singh *et al.* [49] has introduced a finite volume scheme (FVS) whose mathematical formulation is very simple, easy to code and reliably predicts integral moments and number density on a coarse grid. This scheme focuses solely on the conservation of the total mass in the system, but for certain real-life applications, the preservation of the total number of particles is equally important. The problem of non-preservation of the total number of particles has been addressed by Kumar *et al.* [22] extending the scheme of Singh *et al.* [49] which not only preserves the total mass in the system but also preserves the total number of particles in the system. On the other hand, Saha *et al.* [39] developed a mass conserving as well as number preserving finite volume schemes for solving a pure fragmentation PBE. Now the question arises whether these numerical schemes will be stable enough (in terms of discretization errors) when extended to solve a one-dimensional simultaneous coagulation-fragmentation mechanisms? How these numerical schemes behave when extended to a approximate multidimensional population balance equation?

In the literature, it has been shown that the solution of simultaneous coagulation-fragmentation PBE produces significant uncertainty, leading to significant discretization errors, and thus a very refined grid is needed to correctly approximate all numerical outcomes, making these methods computationally very costly [25,26,57]. Even a numerical technique developed by Kostoglou and Karabelas [19] for solving a pure coagulation equation when applied in the presence of fragmentation presents new attributes such as the attainment of a steady state or the appearance of a bimodal or multimodal number

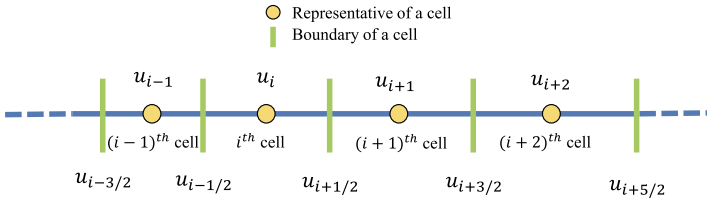

Fig. 2. One-dimensional domain discretization.

density function that was not anticipated. So, Kostoglou and Karabelas [19] made their conclusion by describing it as an inadequate method for solving a simultaneous coagulation-fragmentation PBE.

In comparison to existing sectional methods, the finite volume scheme [11] involves the conversion of the original PBE (1) into the mass conservation form and produces highly inaccurate results of number density function on a coarse grid. Later, Kumar *et al.* [25] developed two methods, namely, one-moment conserving FVS and two-moment conserving FVS. They have shown that when one moment preserving FVS method for coagulation PBE is solved by considering the fragmentation mechanism, it neither holds the preservation of the zeroth moment nor conserve the first order moment. However, the second method is able to conserve the zeroth as well as first order moments but a dense grid is required to predict these results accurately which makes this method computationally very expensive. The mass conservation equation used by Filbet and Laurençot [11] and Kumar *et al.* [25] is given as below:

$$\frac{\partial(un(t,u))}{\partial t} = -\frac{\partial}{\partial u}\Big[\int_0^u \int_{u-v}^{\infty} v\beta(v,v,t)n(t,v)n(t,v)\,dvdv\Big], \quad v,t \in [0,\infty[. \tag{5}$$

Therefore, in this analysis, our primary motivation is to establish two stable (precise and efficient) finite volume approximations for the resolution of one-dimensional simultaneous coagulation-fragmentation PBE. In addition, we also concentrate on extending one-dimensional finite-volume schemes to approximate multidimensional simultaneous coagulation-fragmentation equations to evaluate the effect of discretization errors on numerical solutions. This is because existing schemes when extended to the approximate the higher dimensional population balances, add large values to the discretization errors [37] which was overcome by considering a refined grid. To the best of our knowledge, there is no numerical method available for approximating a 3D simultaneous coagulation-fragmentation equation, however, the extension of the new schemes are done for a 3D PBE in this current work and verified against newly derived integral moments.

Let us now briefly outline the contents of this paper: our exercise begins with a brief introduction of the existing finite volume schemes for pure coagulation as well as pure fragmentation and new methods based on existing methods for solving a simultaneous coagulation-fragmentation PBE are proposed. In same section, the theoretical proofs of the conservation of the moments are provided for both methods. In the next section 3, the developed methods are extended to solve a multidimensional simultaneous coagulation-fragmentation PBE. In section 4.2, the numerical results are discussed and analyzed to verify the accuracy as well as the efficiency of both numerical methods for one, two and three-dimensional PBEs, respectively. Finally, Section 5 summarizes the conclusions of this study.

2. Approximations for one dimensional coagulation-fragmentation

In this part, the mathematical formulations of the proposed finite-volume treatments for the solution of simultaneous coagulation-fragmentation PBE on nonuniform grid are given. The advantage of using nonuniform grid over the uniform grid is shown by Forestier-Coste and Mancini [12]. They have shown that lesser number of nonuniform grid points are required than the nonuniform grid points for achieving the accuracy which reduces the computational expense. The concept behind all numerical methods discussed in this article is based on the premise that the particles inside the grid cell are concentrated on their representatives. For the numerical schemes, a finite one-dimensional computational domain with an upper limit, $u_{max} < \infty$ is taken and divided into I number of smaller cells having u_i as representative volume, for $i \in \{1, 2, ..., I\}$ (see Fig. 2). Now, define the grid points and the step size by

$$u_{1/2} = u_{min}, \quad u_i = \frac{u_{i-1/2} + u_{i+1/2}}{2}, \quad \Delta u_i = u_{i+1/2} - u_{i-1/2}.$$

The goal is to propose two finite volume schemes (a) mass conserving finite volume scheme and (b) number preserving mass conserving for solution of the original PBE (1). Since numerical discretization is used to solve PBE (1), but due to the inclusion of infinity in the integral, it is impossible to solve these problems numerically. Hence, for the implementation of the numerical schemes, the domain must be restricted to $\eta := \{u : u_{min} \le u < u_{max}\}$ and the coagulation kernel is restricted to:

$$\beta(t,u,u') = \begin{cases} \beta(t,u,u'), & (u+u') \le u_{max}; \\ 0, & \text{otherwise.} \end{cases} \tag{6}$$

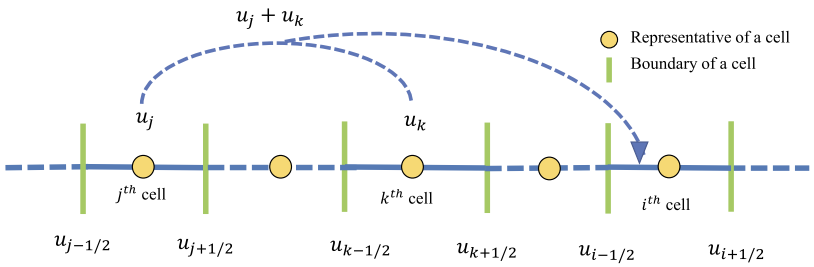

Fig. 3. Representation of set Υ^i.

2.1. *Mass conserving scheme*-MC

In this section, the detail derivation of mathematical formulation of the finite volume mass conservation scheme for the solution of simultaneous coagulation-fragmentation is established. For the numerical approximation, let us first define the following set of indices:

$$\Upsilon^i = \left\{(j,k) \in \mathbb{N} \times \mathbb{N} : u_{i-1/2} < (u_j + u_k) \leq u_{i+1/2}\right\}. \tag{7}$$

Here $u_{i-1/2}$ and $u_{i+1/2}$ are the lower and upper ends of the ith cell, respectively and the representative of the ith cell is u_i (see Fig. 2). The graphical illustration of the Υ^i is shown in Fig. 3. Further, dividing the time domain as $t^{p+1} = t^p + \Delta t^p$ for $p \in \mathbb{N}$. For $i \in 1, 2, ..., I$, assume that n_i^p is the average value of n at time t^p on the cell i which is an approximation of $n(t^p, u_i)$ and is given by the following expression

$$n_i^p = \frac{1}{\Delta u_i} \int_{u_{i-1/2}}^{u_{i+1/2}} n(t^p, u) du. \tag{8}$$

Since we deal with integrals assuming that the point masses are concentrated on representatives, that is, $n(t,u) \approx \sum_{j=1}^{I} N_j \delta(u - u_j)$. Here, N_j denotes the total number of particles in the j^{th} cell. Substituting the approximation of $n(t,u)$ in equation (1) and pursuing the calculations from the work of Kumar *et al.* [23], we define the finite volume scheme as

$$n_i^{p+1} = n_i^p + \Delta t^p \Big(\frac{1}{2} \sum_{i=1}^{I} \sum_{(j,k)\in\Upsilon^i} \beta_{j,k} n_j^p n_k^p \Delta u_j \Delta u_k (u_j + u_k) - \sum_{i=1}^{I} \sum_{j=1}^{I} u_i \beta_{i,j} n_i^p n_j^p \Delta u_i \Delta u_j$$
$$+ \sum_{i=1}^{I} u_i \sum_{k=i}^{I} S_k n_k^p \Delta u_k \int_{u_{i-1/2}}^{g_k^i} b(u, u_k) du - \sum_{i=1}^{I} S_i n_i^p \Big), \tag{9}$$

where

$$g_k^i = \begin{cases} u_i, & \text{if } k = i, \\ u_{i+1/2}, & \text{if } k \neq i. \end{cases}$$

One will observe that the above expression does not hold the mass conservation property. Therefore, some weights defined in equations in the first and fourth terms, respectively are added to the formulation in order to achieve the mass conservation property. Thus, the final expression of MC FVS for solving a simultaneous coagulation-fragmentation equation takes the following form:

$$n_i^{p+1} = n_i^p + \Delta t^p \Big(\frac{1}{2} \sum_{i=1}^{I} \sum_{(j,k)\in\Upsilon^i} \beta_{j,k} n_j^p n_k^p \Delta u_j \Delta u_k (u_j + u_k) \omega_{i,j,k} - \sum_{i=1}^{I} \sum_{j=1}^{I} u_i \beta_{i,j} n_i^p n_j^p \Delta u_i \Delta u_j$$
$$+ \sum_{i=1}^{I} u_i \sum_{k=i}^{I} S_k n_k^p \Delta u_k \int_{u_{i-1/2}}^{g_k^i} b(u, u_k) du - \sum_{i=1}^{I} \Omega_i S_i n_i^p \Big), \tag{10}$$

where

$$\omega_{i,j,k} = \frac{u_j + u_k}{u_i}, \tag{11}$$

$$\Omega_i = \frac{1}{u_i}\sum_{k=1}^{i} u u_k \int_{u_{k-1/2}}^{g_k^i} b(u,u_i)du,\ i=1,2,\cdots,I. \tag{12}$$

To solve these simultaneous processes efficiently, the total birth and total death rates of both processes are considered, that is, we accumulate all those particles who fall in a cell independently of the events that make them appear in the cell. In particular, these events are due to the coagulation and fragmentation processes. Mathematically, the discrete formulation of the simultaneous coagulation-fragmentation problem is obtained as

$$n_i^{p+1} = n_i^p + \Delta t^p \left(B^{\mathrm{MC}}_{coag+frag,i} - D^{\mathrm{MC}}_{coag+frag,i} \right), \tag{13}$$

where the first and second terms on the right side of the equation represent the birth and death of the particles in the ith cell due to the simultaneous coagulation-fragmentation processes and are given a

$$B^{\mathrm{MC}}_{coag+frag,i} = \frac{1}{2}\sum_{i=1}^{I}\sum_{(j,k)\in\Upsilon^i} \beta_{j,k} n_j^p n_k^p \Delta u_j \Delta u_k (u_j+u_k)\omega_{i,j,k} + \sum_{i=1}^{I} u_i \sum_{k=i}^{I} S_k n_k^p \Delta u_k \int_{u_{i-1/2}}^{g_k^i} b(u,u_k)du, \tag{14}$$

and

$$D^{\mathrm{MC}}_{coag+frag,i} = \sum_{i=1}^{I}\sum_{j=1}^{I} u_i \beta_{i,j} n_i^p n_j^p \Delta u_i \Delta u_j + \sum_{i=1}^{I} \Omega_i S_i n_i^p. \tag{15}$$

Next our intent is to prove that the formulation (10) conserves the total mass in the system. The numerical approximation holds the mass conservation property when it satisfies the following condition:

$$\sum_{i=1}^{I} u_i \Delta u_i n_i^{p+1} = \sum_{i=1}^{I} u_i \Delta u_i n_i^p, \text{ for each } p. \tag{16}$$

Proposition 1. *The discrete formulation* (10) *holds the mass conservation property (first order moment) under the restriction* (6)*.*

Proof. Multiplying the discrete formulation provided in equation (10) by $u_i\Delta u_i$ and summing over all i, the left-hand side gives the first order moment at time t^{p+1} and the right-hand side can be evaluated to:

$$\mu_i(t^{p+1}) = \sum_{i=1}^{I} n_i^p u_i \Delta u_i + \Delta t^p T, \tag{17}$$

where

$$T = \frac{1}{2}\sum_{i=1}^{I}\sum_{(j,k)\in\Upsilon^i} \beta_{j,k} n_j^p n_k^p \Delta u_j \Delta u_k (u_j+u_k) + \sum_{i=1}^{I} u_i \sum_{k=i}^{I} S_k n_k^p \Delta u_k \int_{u_{i-1/2}}^{g_k^i} b(u,u_k)du - \sum_{i=1}^{I}\sum_{j=1}^{I} u_i \beta_{i,j} n_i^p n_j^p \Delta u_i \Delta u_j - \sum_{i=1}^{I} \Omega_i S_i n_i^p. \tag{18}$$

In order to prove the mass conservation for simultaneous coagulation-fragmentation PBE, it is required to show that $T = 0$. To prove this, first change the order of the sums in the second term of the right-hand side and using the relation $\int_0^{u_k} u b(u,u_k)du = u_k$, the equation (18) takes the following form:

$$T = \frac{1}{2}\sum_{i=1}^{I}\sum_{j=1}^{I} \beta_{j,k} n_j^p n_k^p \Delta u_j \Delta u_k u_i + \sum_{k=i}^{I} S_k n_k^p \Delta u_k \sum_{i=1}^{I} u_i \int_{u_{i-1/2}}^{g_k^i} b(u,u_k)du - \sum_{i=1}^{I}\sum_{j=1}^{I} u_i \beta_{i,j} n_i^p n_j^p \Delta u_i \Delta u_j - \sum_{i=1}^{I} \Omega_i S_i n_i^p. \tag{19}$$

Using the symmetry property of the coagulation kernel, substituting the value of Ω and interchange the indices in the second (from $k \to i$) and fourth (from $i \to k$) terms, the equation changes to

$$T = \sum_{i=1}^{I}\sum_{j=1}^{I} \beta_{i,j} n_j^p n_i^p \Delta u_j \Delta u_i u_i + \sum_{k=i}^{I} S_k n_k^p \Delta u_k \sum_{i=1}^{I} u_i \int_{u_{i-1/2}}^{g_k^i} b(u,u_k) du$$
$$- \sum_{i=1}^{I}\sum_{j=1}^{I} u_i \beta_{i,j} n_i^p n_j^p \Delta u_i \Delta u_j - \sum_{k=1}^{I} \Omega_k S_k n_k^p. \tag{20}$$

This implies $T = 0$, that is, the total mass of the system is conserved for every time. □

2.2. *Number preserving mass conserving scheme*-NPMC

In this subsection, the mathematical expressions of the number preserving mass conserving finite volume scheme for solving a simultaneous coagulation-fragmentation PBE (1) on non-uniform meshes are provided. In the previous scheme, the major concern of the formulation was to conserve only the total mass in the system. However, the idea of this particular finite volume schemes is based on not only conserving the total mass in the system but also focuses on preserving the total number of particles in the system. The basic concept of this scheme is quite similar to the MC as the same set of indices given in equation (7) are chosen. Hence, by defining the same time discretization, the expression of the formulation can be written as follows:

$$n_i^{p+1} = n_i^p + \frac{\Delta t^p}{2}\left(\sum_{(j,k)\in\Upsilon^i} \beta_{j,k} n_j^p n_k^p \frac{\Delta u_j \Delta u_k}{\Delta u_i} - \sum_{j=1}^{I} \beta_{i,j} n_i^p n_j^p \Delta u_j \right)$$
$$+ \Delta t^p \left(\frac{1}{\Delta u_i} \sum_{k=i}^{I} S_k n_k^p \Delta u_k \int_{u_{i-1/2}}^{g_k^i} b(u,u_k) du - S_i n_i^p \right). \tag{21}$$

Since the main aim of NPMC is to preserve the total number of particles as well as conserve the total mass in the system. However, the expression (21) only gives an account for the preservation of the total number of particles but do not hold mass conservation property. However, this can be achieved easily by introducing four weights into the formulation corresponding to the birth and death terms. Hence, the expression takes the following form:

$$n_i^{p+1} = n_i^p + \Delta t^p \left(\frac{1}{2} \sum_{(j,k)\in\Upsilon^i} \beta_{j,k} n_j^p n_k^p \frac{\Delta u_j \Delta u_k}{\Delta u_i} w_{j,k}^b - \sum_{j=1}^{I} \beta_{i,j} n_i^p n_j^p \Delta u_j w_{i,j}^d \right.$$
$$\left. + \frac{1}{\Delta u_i} \sum_{k=i}^{I} S_k n_k^p \Delta u_k \theta_k^b \int_{u_{i-1/2}}^{g_k^i} b(u,u_k) du - S_i n_i^p \theta_i^d \right). \tag{22}$$

Here $w_{j,k}^b$, $w_{i,j}^d$, θ_k^b and θ_k^b are the weights responsible for the number preservation and mass conservation and are defined as

$$w_{j,k}^b = \begin{cases} \frac{u_j+u_k}{2u_{l_{jk}}-(u_j+u_k)}, & (u_j+u_k) \le u_{max}; \\ 0, & \text{otherwise.} \end{cases}$$

$$w_{i,j}^d = \begin{cases} \frac{u_{l_{ij}}}{2u_{l_{ij}}-(u_i+u_j)}, & (u_i+u_j) \le u_{max}; \\ 0, & \text{otherwise.} \end{cases}$$

$$\theta_k^b = \frac{u_k[v(u_k)-1]}{\sum_k^{i=1}(u_k-u_i)\int_{g_k^i}^{u_{i-1/2}} b(u,u_k)du}, \tag{23}$$

and

$$\theta_i^d = \frac{w_i^b}{u_i} \sum_{k=1}^{i} u_k \int_{u_{k-1/2}}^{g_k^i} b(u, u_i) du. \tag{24}$$

Here l_{jk} denotes the index of the cell where the aggregating particle of the properties $(u_j + u_k)$ falls. Moreover, the index l_{jk} is symmetric with respect to its subindices, that is, $l_{jk} = l_{kj}$. Similar to our previous, the discrete formulation of the NPMC scheme for approximating simultaneous coagulation-fragmentation problem can also be rewritten as

$$n_i^{p+1} = n_i^p + \Delta t^p \left(B^{\text{NPMC}}_{coag+frag,i} - D^{\text{NPMC}}_{coag+frag,i} \right), \tag{25}$$

where the first and second terms on the right side of the equation represent the birth and death of the particles in the ith cell due to the simultaneous coagulation-fragmentation processes and are given as

$$B^{\text{NPMC}}_{coag+frag,i} = \frac{1}{2} \sum_{i=1}^{I} \sum_{(j,k)\in\Upsilon^i} \beta_{j,k} n_j^p n_k^p \Delta u_j \Delta u_k (u_j + u_k) w^b_{j,k} + \sum_{i=1}^{I} u_i \sum_{k=i}^{I} S_k n_k^p \Delta u_k \theta_k^b \int_{u_{i-1/2}}^{g_k^i} b(u, u_k) du, \tag{26}$$

and

$$D^{\text{NPMC}}_{coag+frag,i} = \sum_{i=1}^{I} \sum_{j=1}^{I} u_i \beta_{i,j} n_i^p n_j^p \Delta u_i \Delta u_j w^d_{j,k} + \sum_{i=1}^{I} \Omega_i S_i n_i^p \theta_k^d. \tag{27}$$

Next our purpose is to prove that the formulation (22) preserves zeroth and conserves first order moments. The numerical approximation (22) holds mass conservation under the condition (16) and preserves the number property when it satisfies the following condition:

$$\sum_{i=1}^{\infty} n_i^{p+1} \Delta u_i = \sum_{i=1}^{\infty} n_i^p \Delta u_i - \frac{\Delta t^p}{2} \sum_{i=1}^{I} \sum_{j=1}^{I} \beta^n_{i,j} n_i^p n_j^p \Delta u_i \Delta u_j + \sum_{i=1}^{I} S_i n_i^p \Delta u_i (v(u_i) - 1). \tag{28}$$

The above discrete formulation (28) can be easily retrieved by applying the mid-point quadrature rule to the original continuous PBE (1).

Proposition 2. *The discrete formulation* (22) *holds the mass conservation property (first order moment) under the restriction* (6).

Proof. Multiplying the discrete formulation provided in equation (22) by $u_i \Delta u_i$ and summing over all i similar to the MC FVS, one obtains

$$\mu_1(t^{p+1}) = \sum_{i=1}^{I} n_i^p u_i \Delta u_i + \Delta t^p \widehat{T}, \tag{29}$$

where

$$\widehat{T} = \frac{1}{2} \sum_{i=1}^{I} \sum_{(j,k)\in\Upsilon^i} \beta_{j,k} n_j^p n_k^p \Delta u_j \Delta u_k u_i w^b_{j,k} - \sum_{i=1}^{I} \sum_{j=1}^{I} u_i \beta_{i,j} n_i^p n_j^p \Delta u_i \Delta u_j w^d_{i,j} + \sum_{i=1}^{I} u_i \sum_{k=1}^{I} S_k n_k^p \Delta u_k \theta_k^b \int_{u_{i-1/2}}^{g_k^i} b(u, u_k) du - \sum_{i=1}^{I} u_i S_i n_i^p \Delta u_i \theta_i^d. \tag{30}$$

Similar to the case of the MC FVS, it is required to show $\widehat{T} = 0$ for this discrete formulation. Proceeding as above Proposition 1, first change the order of integration of the sums in the third term of the right hand side will give the following expression:

$$\widehat{T} = \frac{1}{2}\sum_{i=1}^{I}\sum_{(j,k)\in\Upsilon^i}\beta_{j,k}n_j^p n_k^p \Delta u_j \Delta u_k u_i w_{j,k}^b - \sum_{i=1}^{I}\sum_{j=1}^{I} u_i \beta_{i,j}^n n_i^p n_j^p \Delta u_i \Delta u_j w_{i,j}^d + \sum_{i=1}^{I} S_i n_i^p \Delta u_i \Big(\theta_i^b \sum_{k=1}^{i} u_k \int_{u_{k-1/2}}^{g_k^i} b(u,u_k)du - \theta_i^d\Big). \tag{31}$$

Further, rearranging the terms using the symmetry of the kernel and l_{ij}, the following can be achieved:

$$\begin{aligned}\widehat{T} =& \frac{1}{2}\sum_{i=1}^{I}\sum_{j=1}^{I}\beta_{i,j}n_j^p n_i^p \Delta u_j \Delta u_i \frac{u_i u_{l_{ij}}}{2u_{l_{ij}} - (u_i+u_j)} - \sum_{i=1}^{I}\sum_{j=1}^{I}\beta_{i,j}^n n_i^p n_j^p \Delta u_i \Delta u_j \frac{u_i u_{l_{ij}}}{2u_{l_{ij}} - (u_i+u_j)} \\ &+ \sum_{i=1}^{I} S_k n_k^p \Delta u_k \Big(\sum_{k=1}^{k} u_i \int_{u_{i-1/2}}^{g_k^i} b(u,u_k)du - u_k \frac{1}{u_k}\sum_{i=1}^{k} u_i \int_{u_{i-1/2}}^{g_i^k} b(u,u_k)du\Big) \\ &= 0.\end{aligned} \tag{32}$$

This clearly signifies that the NPMC FVS does hold the mass conservation property of the system. □

Proposition 3. *The discrete formulation* (22) *holds the number preservation property (zeroth order moment) under the restriction* (6)*.*

Proof. Multiplying the discrete formulation provided in equation (22) by Δu_i and summing over all i leads to the following relation

$$\mu_1(t^{p+1}) = \sum_{i=1}^{I} n_i^p u_i \Delta u_i + \Delta t^p \widehat{T}_1, \tag{33}$$

where

$$\widehat{T}_1 = \frac{1}{2}\sum_{i=1}^{I}\sum_{j=1}^{I}\beta_{i,j}n_j^p n_i^p \Delta u_j \Delta u_i w_{i,j}^b - \sum_{i=1}^{I}\sum_{j=1}^{I}\beta_{i,j}n_i^p n_j^p \Delta u_i \Delta u_j w_{i,j}^d + \sum_{i=1}^{I}\sum_{k=i}^{I} S_i n_i^p \Delta u_i \theta_i^b \int_{u_{i-1/2}}^{g_k^i} b(u,u_k)du - \sum_{i=1}^{I} S_i n_i^p \Delta u_i \theta_i^d. \tag{34}$$

Combining the first-two summations and substituting the values of weights, we have

$$\widehat{T}_1 = \frac{1}{2}\sum_{i=1}^{I}\sum_{j=1}^{I}\beta_{i,j}n_j^p n_i^p \Delta u_j \Delta u_i \Big(\frac{u_i+u_j}{2u_{l_{ij}} - (u_i+u_j)} - \frac{u_{l_{ij}}}{2u_{l_{ij}} - (u_i+u_j)}\Big) + \sum_{i=1}^{I} S_i n_i^p \Delta u_i \times \frac{u_i[v(u_i)-1]}{\sum_{k=1}^{i}(u_i-u_k)\int_{g_k^i}^{u_{k-1/2}} b(u,u_i)du}\Big(\sum_{k=1}^{i}(u_i-u_k)\int_{g_k^i}^{u_{k-1/2}} b(u,u_i)du\Big). \tag{35}$$

On simplification, the above gives

$$\widehat{T}_1 = -\frac{1}{2}\sum_{i=1}^{I}\sum_{j=1}^{I}\beta_{i,j}n_j^p n_i^p \Delta u_j \Delta u_i + \sum_{i=1}^{I} S_i n_i^p \Delta u_i \frac{u_i[v(u_i)-1]}{\sum_{k=1}^{i}(u_i-u_k)\int_{g_k^i}^{u_{k-1/2}} b(u,u_i)du} \times \Big(\sum_{k=1}^{i}(u_i-u_k)\int_{g_k^i}^{u_{k-1/2}} b(u,u_i)du\Big). \tag{36}$$

This implies

$$\widehat{T}_1 = -\frac{1}{2}\sum_{i=1}^{I}\sum_{j=1}^{I}\beta_{i,j}n_j^p n_i^p \Delta u_j \Delta u_i + \sum_{i=1}^{I} S_i n_i^p \Delta u_i (v(u_i) - 1). \tag{37}$$

Hence the NPMC FVS is also preserving the total number property of the system along with its mass conservation property. □

3. Approximations for multidimensional coagulation-fragmentation

Before dealing with the validation of the numerical methods for a one-dimensional PBE, let us first give the generalized formulations for approximating a multidimensional simultaneous coagulation-fragmentation PBE. Define $\mathbb{R}_+^d$ the space of vectors $\vec{u} = [u_1, u_2, \ldots, u_d]^T$ of length d, such that $u_k \geq 0$ for all $k = 1, 2, \ldots, d$. The multidimensional population balance model incorporating simultaneous coagulation-fragmentation processes can be written as follows:

$$\frac{\partial n(t,\vec{u})}{\partial t} = Q_{agg}^{\pm}(t,\vec{u}) + Q_{brk}^{\pm}(t,\vec{u}), \tag{38}$$

with initial condition $n(0,\vec{u}) = n_0(\vec{u})$, $\vec{u} \in \mathbb{R}_+$, where, $(t,\vec{u}) \in \mathbb{R}_+^2$ and $\mathbb{R}_+ := (\vec{0}, \vec{\infty})$. The finite dimensional vector $\vec{u}$ denotes the state vector in terms of additive properties like mass or volume. Moreover,

$$Q_{agg}^{\pm}(t,\vec{u}) = \frac{1}{2}\int_{\vec{0}}^{\vec{u}} \beta(t,\vec{u}-\vec{u}',\vec{u}')n(t,\vec{u}-\vec{u}')n(t,\vec{u}')d\vec{u}' - \int_{\vec{0}}^{\vec{\infty}} \beta(t,\vec{u},\vec{u}')n(t,\vec{u})n(t,\vec{u}')d\vec{u}', \tag{39}$$

and

$$Q_{brk}^{\pm}(t,\vec{u}) = \int_{\vec{u}}^{\vec{\infty}} b(\vec{u},\vec{u}')S(\vec{u}')n(t,\vec{u}')d\vec{u}' - S(\vec{u})n(t,\vec{u}), \tag{40}$$

where $\beta(t,\vec{u},\vec{u}')$, $b(\vec{u},\vec{u}')$ and $S(\vec{u})$ defines the aggregation kernel, breakage kernel and selection function, respectively similar to the one-dimensional case and $d\vec{u} = \prod_{k=1}^{d} du_k$.

The multidimensional moment of order $p = \sum_{r=1}^{d}\lambda_r$ is defined by

$$\mu_{\lambda_1,\lambda_2,\ldots,\lambda_d}(t) = \int_{\vec{0}}^{\vec{\infty}} \prod_{k=1}^{d} u_k^{\lambda_k} n(t,\vec{u})d\vec{u}. \tag{41}$$

Choosing $\lambda_k = 0$ for every k will give the zeroth order moment whereas the first order moment $\mu_{0,\ldots1,\ldots,0}(t)$ (1 in kth position) is the total value (mass) of the kth property.

Before providing the formulations of the finite volume schemes for solving the multidimensional population balance model incorporating simultaneous coagulation-fragmentation, first it required to define the computational domain. The multidimensional computational domain with the limits $\vec{u}_{min}$ and $\vec{u}_{max}$ is divided into I number of cells in the computational domain. For any cell i, the lower and upper boundaries of the cell are denoted by $\vec{u}_{i-1/2}$ and $\vec{u}_{i+1/2}$ respectively. The representative of the cell i is $\vec{u}_i = [u_{i_1}, u_{i_2}, \ldots, u_{i_d}]^T$ where $u_{i_r} = \dfrac{u_{i_r-1/2} + u_{i_r+1/2}}{2}$ with the usual assumption $\vec{u}_{1_r-1/2} = \vec{u}_{min}$ for each r.

Similar to one case, here we also develop two finite volume schemes for the multidimensional PBE (38). Proceeding as previous cases, assume that n_i^p for $i \in 1, 2, \ldots, I$ is the average value of n at time t^p on the ith cell which is an approximation of $n(t^p, \vec{u}_i)$ and is given by

$$n_i^p = \frac{1}{\Delta\vec{u}_i}\int_{\vec{u}_{i-1/2}}^{\vec{u}_{i+1/2}} n(t^p,\vec{u})d\vec{u}. \tag{42}$$

For the multidimensional case, it is also assumed that the point masses are concentrated on representatives, that is, $n(t,\vec{u}) \approx \sum_{j=1}^{I} N_j \delta(\vec{u} - \vec{u}_j)$. Substituting this expression in equation (38) and using the indices defined in equation (7) will give us the following expression:

$$n_i^{p+1} = n_i^p + \Delta t^p \Big(\frac{1}{2}\sum_{(j,k)\in\Upsilon^i} \beta(\vec{u}_j,\vec{u}_k)n_j^p n_k^p \frac{\Delta\vec{u}_j \Delta\vec{u}_k}{\Delta\vec{u}_i} - \sum_{j=1}^{I}\beta(\vec{u}_i,\vec{u}_j)\, n_i^p\, n_j^p \Delta\vec{u}_j$$

$$+\frac{1}{\Delta\vec{u}_i}\sum_{k=i}^{I} S_k n_k \Delta\vec{u}_k \int_{\vec{u}_{i-1/2}}^{g_k^i} b(\vec{u},\vec{u}_k)d\vec{u} - S_i n_i\Big). \tag{43}$$

It can be observed that the above formulation is not mass conserving as it is the essential criteria for any numerical method. Therefore, the following weights are added to make the formulation mass conserving:

$$\omega_{i,j,k} = \frac{\vec{u}_j + \vec{u}_k}{\vec{u}_i}, \tag{44}$$

and

$$\Omega_i = \frac{1}{\vec{u}_i}\sum_{k=1}^{i} \vec{u}\vec{u}_k \int_{\vec{u}_{k-1/2}}^{g_k^i} b(\vec{u},\vec{u}_i)d\vec{u},\ i = 1,2,\cdots,I, \tag{45}$$

where

$$g_k^i = \begin{cases} \vec{u}_i, & \text{if } k = i, \\ \vec{u}_{i+1/2}, & \text{if } k \neq i. \end{cases}$$

By adding the weights in the equation (43) will take the following form:

$$n_i^{p+1} = n_i^p + \Delta t^p\Big(\frac{1}{2}\sum_{(j,k)\in\Upsilon^i} \beta(\vec{u}_j,\vec{u}_k) n_j^p n_k^p \frac{\Delta\vec{u}_j\Delta\vec{u}_k}{\Delta\vec{u}_i}\omega_{i,j,k} - \sum_{j=1}^{I}\beta(\vec{u}_i,\vec{u}_j)\, n_i^p\, n_j^p \Delta\vec{u}_j$$
$$+\frac{1}{\Delta\vec{u}_i}\sum_{k=i}^{I} S_k n_k \Delta\vec{u}_k \int_{\vec{u}_{i-1/2}}^{g_k^i} b(\vec{u},\vec{u}_k)d\vec{u}\Omega_i - S_i n_i\Big). \tag{46}$$

This formulation is only focusing on the conservation of the total mass in the system but does not responsible for the preservation of the total number of particles (zeroth order moment). The theoretical proof of the mass conservation property is similar to the case described in Proposition 1 of section 2.1.

Further our intention will be to derive a formulation for the multidimensional PBE (38) which holds both preservation of zeroth order moment and conservation of first order moment. This can be done easily by adding the following weights to the formulation (43):

$$w_{i,j}^d = \begin{cases} \dfrac{\vec{u}_j + \vec{u}_k}{2\vec{u}_{l_{jk}} - (\vec{u}_j + \vec{u}_k)}, & (\vec{u}_i + \vec{u}_j) \le \vec{u}_{max}; \\ 0, & \text{otherwise.} \end{cases} \tag{47}$$

$$w_{i,j}^d = \begin{cases} \dfrac{\vec{u}_{l_{ij}}}{2\vec{u}_{l_{ij}} - (\vec{u}_i + \vec{u}_j)}, & (\vec{u}_i + \vec{u}_j) \le \vec{u}_{max}; \\ 0, & \text{otherwise.} \end{cases} \tag{48}$$

and

$$\theta_k^b = \frac{\vec{u}_k[\nu(\vec{u}_k) - 1]}{\sum_k^{i=1}(\vec{u}_k - \vec{u}_i)\int_{g_k^i}^{\vec{u}_{i-1/2}} b(\vec{u},\vec{u}_k)d\vec{u}}, \tag{49}$$

$$\theta_i^d = \frac{w_i^b}{\vec{u}_i}\sum_{k=1}^{i}\vec{u}_k \int_{\vec{u}_{k-1/2}}^{g_k^i} b(\vec{u},\vec{u}_i)d\vec{u}. \tag{50}$$

Further substituting the weights $w_{i,j}^d$, $w_{i,j}^b$, θ_k^b and θ_k^d in the formulation (43) will give the final expression of the number preserving mass conserving discrete formulation is given by

$$n_i^{p+1} = n_i^p + \Delta t^p\left(\frac{1}{2}\sum_{(j,k)\in\Upsilon^i}\beta(\vec{u}_j,\vec{u}_k) n_j^p n_k^p \frac{\Delta\vec{u}_j\Delta\vec{u}_k}{\Delta\vec{u}_i} w_{i,j}^d - \sum_{j=0}^{I}\beta(\vec{u}_i,\vec{u}_j)\, n_i^p\, n_j^p \Delta\vec{u}_j w_{i,j}^b\right.$$

$$+\frac{1}{\Delta\vec{u}_i}\sum_{k=i}^{I} S_k n_k \Delta\vec{u}_k \theta_k^b \int_{\vec{u}_{i-1/2}}^{g_k^i} b(\vec{u},\vec{u}_k) d\vec{u}\Omega_i - S_i n_i \theta_k^d \Bigg). \tag{51}$$

The theoretical proofs of the integral properties such as preservation of total number of particles and conservation of total mass in the system are similar to the proofs provided in Propositions 2 & 3 of section 2.2.

Since we are working with an explicit discrete methods, therefore, it is meaningful to impose some constraints on time step to ensure positivity of the solution (often called the CFL condition). Similar to the condition proposed by Filbet and Laurençot [11], the following constraint on the time step ensures the positivity of the solution:

$$\Delta t^p < \min_i \left(\left| \frac{n_i^p}{B_i^p - D_i^p} \right| \right). \tag{52}$$

Here B_i^p and D_i^p are discrete birth and death terms at time t^p, respectively of the numerical methods described in sections 2.1, 2.2 and 3.

4. Results and discussions

In order to validate the efficiency and accuracy of the numerical schemes, the numerical results predicted by both MC and NPMC schemes are compared with the existing cell average technique [23] and the exact results for analytically tractable kernels. To show the accuracy of numerical methods, the quantitative relative errors [44,48,53–55] in the different order moments (corresponding to analytically tractable kernels) for different number of grid points are also calculating using:

$$\Delta_i(t) = \left| \frac{\mu_i^{exc} - \mu_i^{num}}{\mu_i^{exc}} \right|. \tag{53}$$

The superscripts *exc* and *num* represent the exact and numerical solutions, respectively. Here, Δ_0 and Δ_1 denote the relative errors in zeroth order moment (total number of particles) and first order moment (total mass of the system), respectively. It is significant to note that the relative errors in the various order moments are calculated at the end of the simulations (end time). The computations for all schemes were carried out using `MATLAB` on a `i5` 7th generation CPU with 2.40 `GHz` and 16 `GB RAM`.

4.1. Simultaneous coagulation-fragmentation-1D

In this part of the paper, the numerical results obtained by solving a simultaneous coagulation-fragmentation PBE are compared with the exact results corresponding to various combination of coagulation kernel and selection functions. In particular, four various combinations of coagulation kernel and selection functions are considered:

Case (a): Constant coagulation kernel and constant selection function.
Case (b): Constant coagulation kernel and linear selection function.
Case (c): Multiplicative coagulation kernel and constant selection function.
Case (d): Multiplicative coagulation kernel and linear selection function.

For every combination, a binary fragmentation kernel is considered. The exact solution of the number density function for a simultaneous coagulation-fragmentation PBE were derived by Patil and Andrews [32] corresponding to a constant coagulation kernel and linear selection function with binary breakage kernel. For the other combinations, there is no availability of the number density function in the literature, hence, the comparison is conducted only for zeroth and first order moments and their analytical (or exact) results were derived by Kumar *et al.* [25].

4.1.1. Case (a): *constant coagulation kernel and constant selection function*

For a simultaneous coagulation-fragmentation PBE, the comparison of numerical results with the exact results is conducted for a constant coagulation kernel and constant selection function. The domain considered to run the simulations consist of particles sized from $u_{min} = 10^{-3}$ to $u_{max} = 200$, divided into 30 nonuniform cells, whereas the time taken to run the simulations is 0 to 18.

Fig. 4 shows the comparison of the numerical results and exact results for a combination of constant coagulation kernel and constant selection function. Since the exact solution of number density function is not available in literature. Therefore, the accuracy of the numerical methods is verified by comparing with the exact zeroth and first order moments. One can observe that the zeroth and first order moments approximated by NPMC and cell average technique (CAT) overlap with the exact results, however, the MC shows underprediction for the zeroth order moment. This is because the MC do not give any account for the preservation of the zeroth order moment, whereas both NPMC and CAT preserves the zeroth order moment along with the conservation of the first order moment. Moreover, if the number of grid points in a given domain increases,

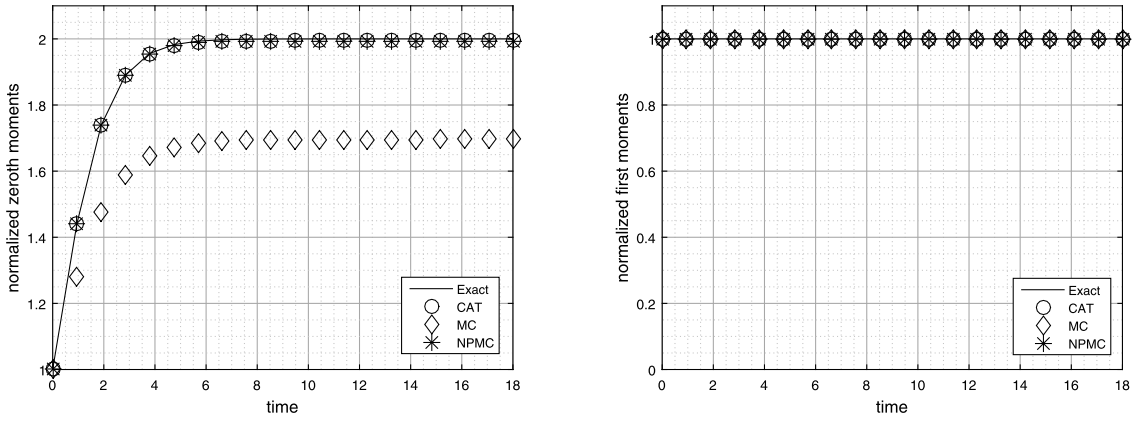

(a) Zeroth order moment (μ_0) (b) First order moment (μ_1)

Fig. 4. Comparison of various order moments for constant coagulation kernel and constant selection function.

Table 1
Relative errors in various order moments for constant coagulation kernel and constant selection function.

Δ	CAT 30 cells	MC 30 cells	NPMC 30 cells	CAT 50 cells	MC 50 cells	NPMC 50 cells
Δ_0	0.05391	0.15736	0.05359	0.05341	0.09419	0.05144
Δ_1	9.14×10^{-10}	6.18×10^{-10}	5.81×10^{-12}	3.91×10^{-10}	1.59×10^{-10}	0.00000

Table 2
CPU time taken by numerical methods using constant coagulation kernel and constant selection function.

Method	Cells	Time taken (in seconds)	Cells	Time taken (in seconds)
MC	30	0.3865	50	0.5091
NPMC	30	0.3635	50	0.4669
CAT	30	0.4598	50	0.6927

Table 3
Relative errors in various order moments for constant coagulation kernel and linear selection function.

Δ	CAT 30 cells	MC 30 cells	NPMC 30 cells	CAT 50 cells	MC 50 cells	NPMC 50 cells
Δ_0	0.02303	0.10433	0.02303	0.01341	0.04419	0.01044
Δ_1	1.55×10^{-15}	1.22×10^{-15}	9.99×10^{-16}	3.44×10^{-16}	8.88×10^{-16}	2.88×10^{-16}

the results obtained by the MC scheme certainly improve to higher extent, however adds value to the computational time. This can be verified in Table 1, quantitatively. It shows that the relative errors in zeroth and first order moments improve when a refined grid is used. It is also interesting to see that the number of particles are increasing till time $t = 4$ as the combination of binary fragmentation kernel and constant selection function is dominating the constant coagulation kernel (see Fig. 5(e)). After time $t = 4$, the system acquires the steady-state solution.

In addition, the comparison of the all numerical methods is also done in terms of the computational CPU time. Table 2 shows that the NPMC and MC obtained the various results more efficiently than the CAT. However, among NPMC and MC, the NPMC took lesser time to compute these numerical results than the MC.

4.1.2. Case (b): *constant coagulation kernel and linear selection function*

Further the comparison of the numerical results obtained with the constant coagulation kernel and linear selection function are compared with the exact results. The computational domain considered for the numerical simulations is same as the previous case. Fig. 5 illustrates the comparison of the numerical results with the exact results for this particular case. It is shown that the zeroth order moments computed by NPMC and CAT agree very well with the exact moment, whereas similar to the previous case, the zeroth order moment obtained by the MC method shows underprediction from the exact moment. Moreover, the first order moments approximated by all numerical methods coincide with the exact result. In addition, the number density function plotted at different times computed using all numerical methods show equal accuracy, that is, the numerical results overlap with the exact results.

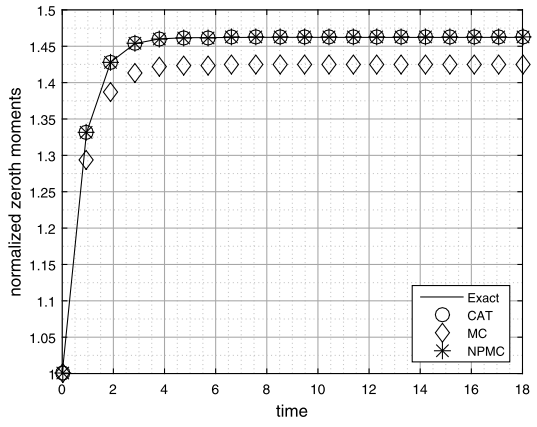

(a) Zeroth order moment (μ_0)

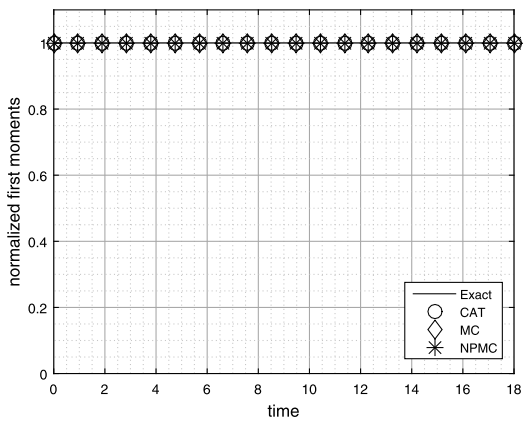

(b) First order moment (μ_1)

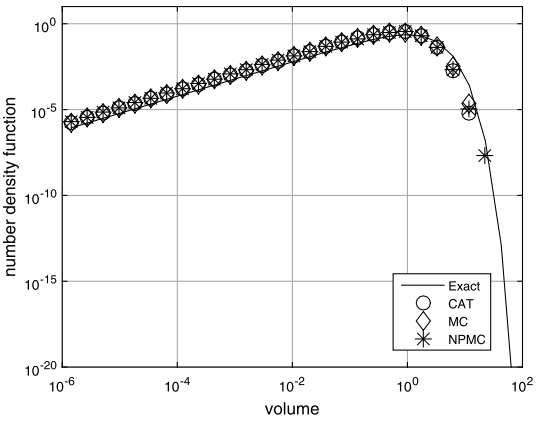

(c) Number density at $t = 8.52$

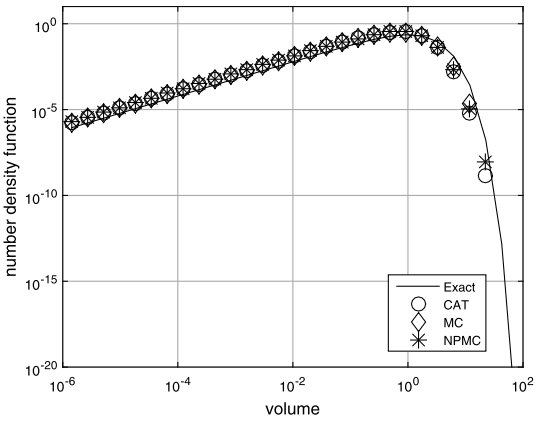

(d) Number density at $t = 13.26$

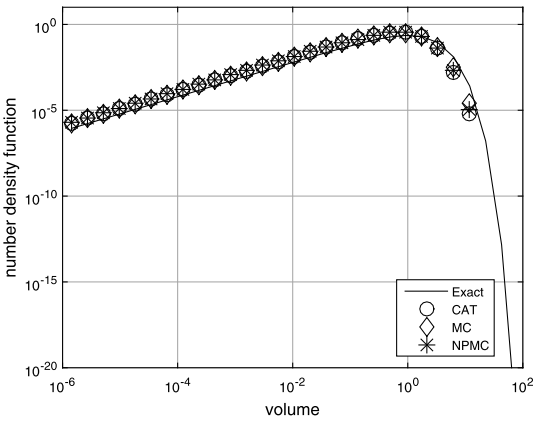

(e) Number density at $t = 18$

Fig. 5. Comparison of various order moments and number density for constant coagulation kernel and linear selection function.

Table 4
CPU time taken by numerical methods using constant coagulation kernel and linear selection function.

Method	Cells	Time taken (in seconds)	Cells	Time taken (in seconds)
MC	30	0.8298	50	1.2558
NPMC	30	0.7442	50	1.0727
CAT	30	0.9373	50	1.9820

Table 5
Relative errors in various order moments for multiplicative coagulation kernel and constant selection function.

Δ	CAT 30 cells	MC 30 cells	NPMC 30 cells	CAT 50 cells	MC 50 cells	NPMC 50 cells
Δ_0	0.11673	0.15000	0.10099	0.10650	0.08783	0.05144
Δ_1	0.16233	0.04717	0.07102	0.04230	0.03789	0.03770

Table 6
CPU time taken by numerical methods using multiplicative coagulation kernel and constant selection function.

Method	Cells	Time taken (in seconds)	Cells	Time taken (in seconds)
MC	30	0.3685	50	0.4751
NPMC	30	0.2608	50	0.3301
CAT	30	0.4066	50	0.7947

In addition, the relative errors existed in the various order moments calculated by all numerical methods are illustrated in Table 3. As expected, the NPMC shows less errors in the zeroth and first order moments than both MC and CAT. Moreover, in terms computational aspect, the NPMC method calculated the numerical results by consuming lesser CPU time than the other methods on coarse as well as refined grids (see Table 4). Additionally, the MC method is also more efficient than the CAT.

4.1.3. Case (c): *multiplicative coagulation kernel and constant selection function*

To enhance the comparison, a more complex coagulation kernel (multiplicative kernel, $\beta(u, u') = uu'$) is considered with the constant selection function. The multiplicative kernel is well known as a gelling kernel, that is, a state that occurs for certain coagulation kernels where mass is lost from particles of finite size and appears in particles of infinite size Ernst *et al.* [9] The computational grid taken from $u_{min} = 10^{-10}$ to $u_{max} = 10^3$ is divided into 30 and 50 non-uniform cells and the simulations are run from time 0 to 0.45. The comparison of the numerical results and exact results corresponding to a multiplicative coagulation kernel and constant selection function can be seen in Fig. 6. The exact results of zeroth and first order moments are provided in Kumar *et al.* [25]. The zeroth order moment approximated by the NPMC shows very good agreement with the exact moment where both CAT and MC show overproduction and underprediction from the exact result, respectively. Moreover, the first order moment predicted by both MC and NPMC methods show comparative results but on the other side the CAT started to lose mass after time $t = 0.325s$ (see Fig. 6(b)). Additionally, the second order moments predicted by both finite volume schemes show better accuracy than the CAT as the existing method deviates significantly from the exact solution, refer to Fig. 6(c). However, these numerical results can be improved to desired values by choosing a more refined grid as demonstrated in Fig. 7. It can be seen that the different order moments compared in Figs. 7(a), 7(b) and 7(c) improve to large extent when a nonuniform grid of 50 cells is used. However, still, the second order moments computed by both MC and NPMC show better results than the CAT, see Fig. 7(c). In addition, the relative error in various order moments is shown in Table 5 for a computational grid consist of 30 and 50 nonuniform cells. It can be observed that the relative errors in the moments approach almost equal values on a refined grid for all numerical methods. But, in terms of computational time, the NPMC and MC are highly efficient methods in calculating the numerical results as compared to the CAT on both coarse and refined grids as shown in Table 6.

4.1.4. Case (d): *multiplicative coagulation kernel and linear selection function*

Here, a comparison of the numerical results corresponding to multiplicative coagulation kernel and linear selection function is shown with the exact results. The grid considered and time taken to run the simulations is similar to the previous case.

Fig. 8 demonstrates the comparison of the moments predicted using the numerical methods with the exact moments. The exact results for zeroth as well as first order moments were derived by Kumar *et al.* [25] for this particular case. The zeroth and first order moments predicted by both NPMC and CAT are showing a very good agreement with the exact moments. However, as expected the zeroth order moment predicted by the MC shows underprediction from the exact result. Moreover, all numerical results show very good agreement for the first order moments.

In order to check the accuracy of this case on a refined grid, the relative errors existed in the moments are calculated and listed in Table 7. The similar trend to the previous case is obtained by the moments as the NPMC calculated these

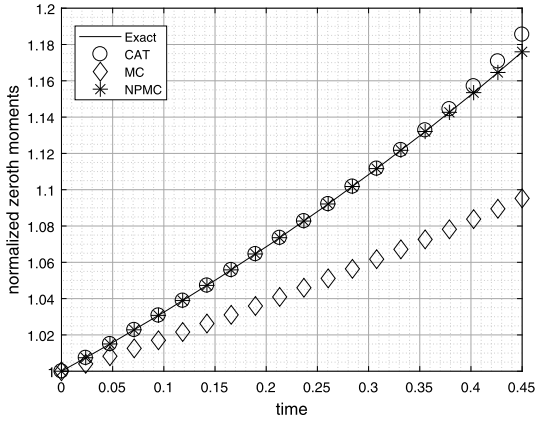

(a) Zeroth order moment (μ_0)

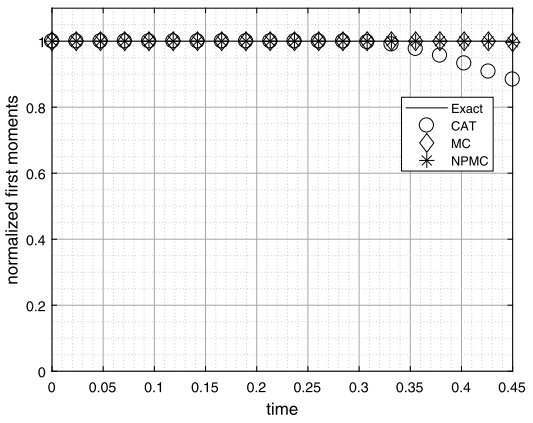

(b) First order moment (μ_1)

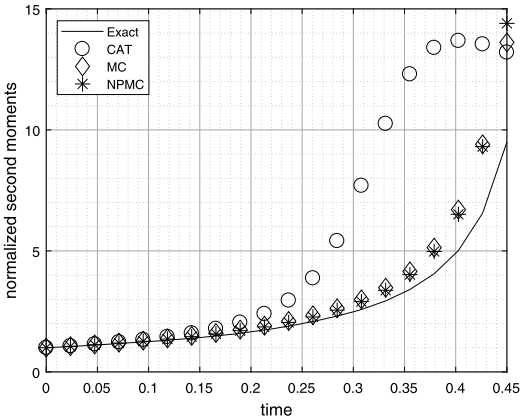

(c) Second order moment (μ_2)

Fig. 6. Comparison of various order moments for multiplicative coagulation kernel and constant selection function using 30 nonuniform cells.

Table 7
Relative errors in various order moments for multiplicative coagulation kernel and linear selection function.

Δ	CAT 30 cells	MC 30 cells	NPMC 30 cells	CAT 50 cells	MC 50 cells	NPMC 50 cells
Δ_0	0.16165	0.10807	0.10807	0.05341	0.09419	0.05144
Δ_1	2.2×10^{-15}	1.3×10^{-15}	3.7×10^{-16}	1.8×10^{-16}	1.3×10^{-16}	0.00000

Table 8
CPU time taken by numerical methods using constant coagulation kernel and linear selection function.

Method	Cells	Time taken (in seconds)	Cells	Time taken (in seconds)
MC	30	0.2047	50	0.3358
NPMC	30	0.1755	50	0.3178
CAT	30	0.4604	50	0.9181

errors with more precision than the other two methods. Also, from Table 8, it is easy to observe that the NPMC method predicted these results by consuming lesser CPU time than both MC and CAT.

Finally, it can be concluded that the NPMC method is the highly accurate and efficient method for approximating a one-dimensional simultaneous coagulation-fragmentation equation.

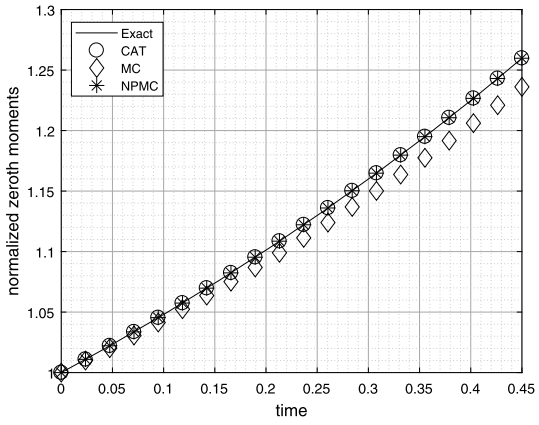

(a) Zeroth order moment (μ_0)

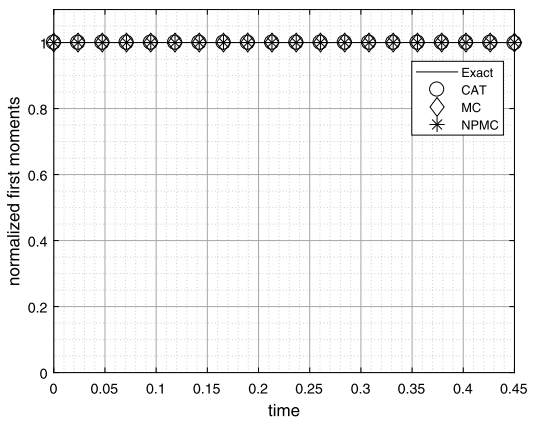

(b) First order moment (μ_1)

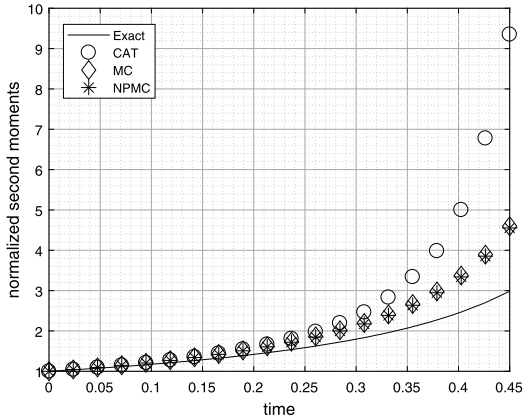

(c) Second order moment (μ_2)

Fig. 7. Comparison of various order moments for multiplicative coagulation kernel and constant selection function using 50 nonuniform cells.

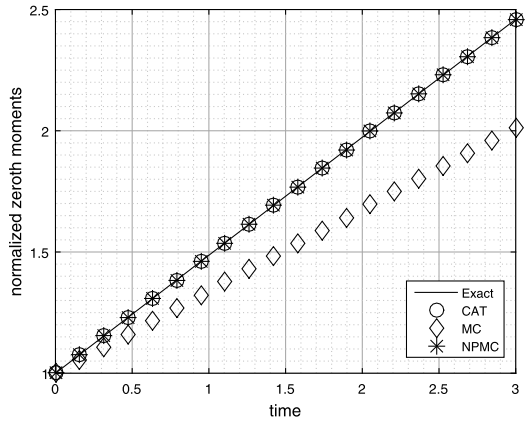

(a) Zeroth order moment (μ_0)

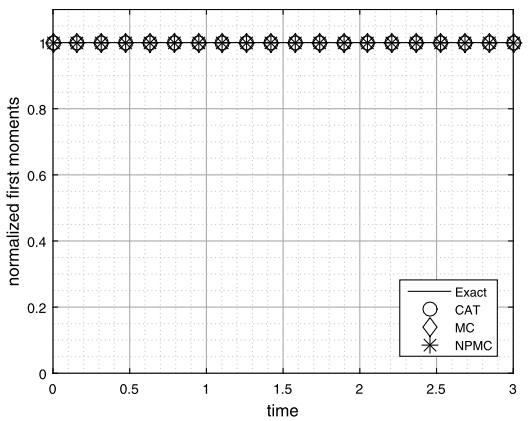

(b) First order moment (μ_1)

Fig. 8. Comparison of various order moments for multiplicative coagulation kernel and linear selection function.

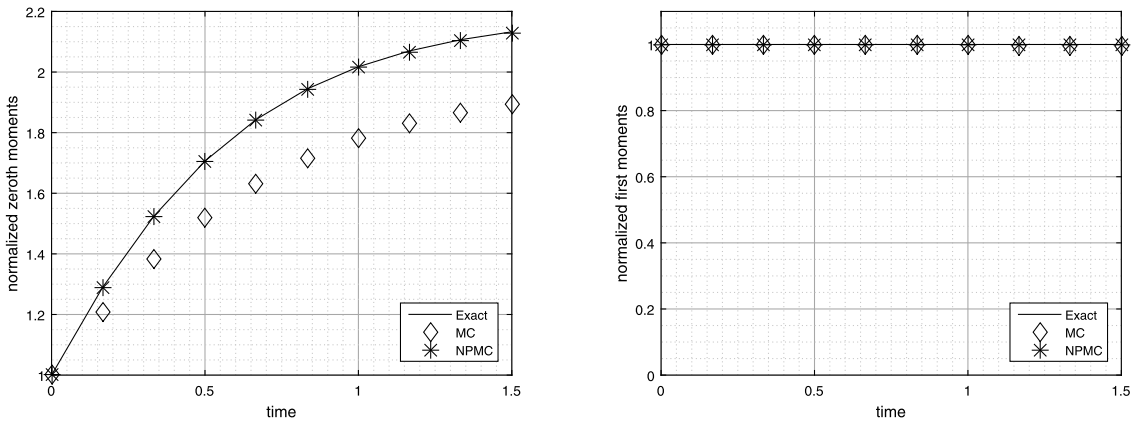

(a) Zeroth order moment ($\mu_{0,0}$) (b) First order moment ($\mu_{1,0} + \mu_{0,1}$)

Fig. 9. Comparison of various order moments for a constant coagulation kernel and linear selection function.

Table 9
Relative errors in various order moments for constant coagulation kernel and linear selection function.

Δ	MC 400 cells	NPMC 400 cells	MC 525 cells	NPMC 525 cells
Δ_0	0.1111	0.0012	0.0567	8.14×10^{-04}
Δ_1	2.09×10^{-15}	2.09×10^{-15}	1.30×10^{-16}	1.33×10^{-16}

4.2. Simultaneous coagulation-fragmentation-2D

This section is devoted to comparing the results of both MC and NPMC for approximating a multidimensional simultaneous coagulation-fragmentation PBE with the exact results corresponding to different combinations of coagulation kernels and selection functions. In particular, the following combination is considered for the comparison:

Case (1): Constant coagulation kernel and linear selection function.
Case (2): Additive coagulation kernel and constant selection function.

Similar of the one-dimensional case, for the multidimensional cases the binary breakage kernel is considered. It can be observed in the literature that for the multidimensional PBE, the exact results are neither available for the number density functions nor the different order moments corresponding to any combination of coagulation-fragmentation kernels. In this work, the accuracy of the methods is verified by deriving the new exact results of zeroth as well as first order moments for Case (1) and Case (2). Even though the formulations of the numerical methods are provided for approximating the multidimensional simultaneous coagulation-fragmentation PBE but the verification is only done by considering a two-dimensional PBE as the exact solutions for moments are difficult to derive for higher dimensional PBE's. The complete derivation of the exact moments obtained by solving a two-dimensional PBE can be found in Appendix A.

4.2.1. Case (1): *constant coagulation kernel and linear selection function*

In this section, the comparison numerical zeroth and first order moments with exact results is conducted using constant coagulation kernel and linear selection function. The computational grid taken for conducting is taken from $\vec{u}_{min} = 10^{-6}$ to $\vec{u}_{max} = 3 \times 10^3$ is divided into 20 non-uniform cells along both directions for a two-dimensional PBE, that is, a grid of 400 nonuniform cells is considered. However, the simulations are run until time $t = 1.5$.

Fig. 9 demonstrates the comparison of zeroth and first order moments predicted numerically and analytically (or exact). As expected, the zeroth order moment computed by the NPMC method shows excellent agreement with the exact moment whereas, the zeroth order moment computed using the MC method exhibits underprediction from the exact moment. However, the first order moment captured very well by both numerical methods and overlaps with the exact moment. In addition, the relative errors existed in the moments are quantified in Table 9. It also reveals that the errors obtained in both moments using NPMC are lesser than the MC. However, if a more refined grid is used then the errors in the moments can be reduced to a desired level. Moreover, the time required to compute the numerical results by both numerical methods is listed in Table 10. It reveals that the NPMC is more efficient than the MC as it took less CPU time to compute the numerical results.

Table 10
CPU time taken by numerical methods using constant coagulation kernel and linear selection function.

Method	Cells	Time taken (in seconds)	Cells	Time taken (in seconds)
MC	400	35.67	525	78.01
NPMC	400	35.15	525	77.81

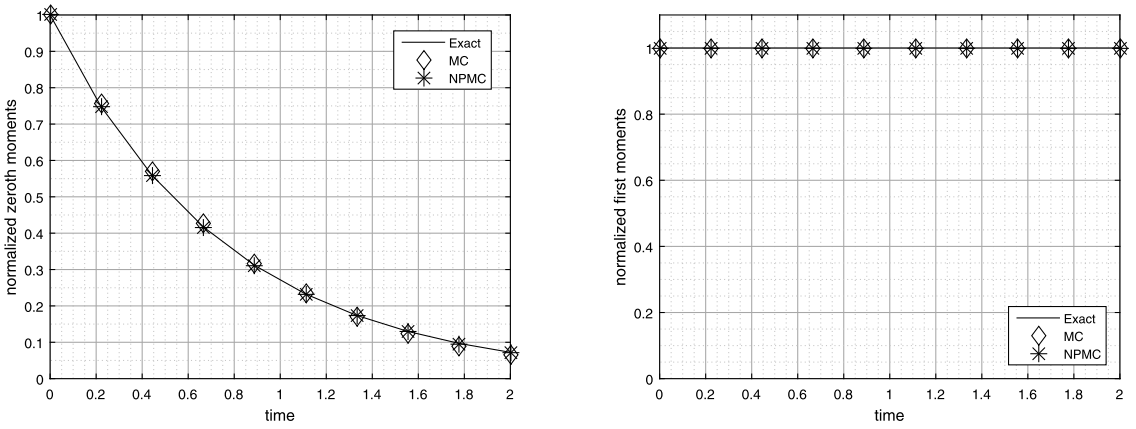

(a) Zeroth order moment ($\mu_{0,0}$) (b) First order moment ($\mu_{1,0} + \mu_{0,1}$)

Fig. 10. Comparison of various order moments for additive coagulation kernel and constant selection function.

Table 11
Relative errors in various order moments for constant coagulation kernel and linear selection function.

Δ	MC 400 cells	NPMC 400 cells	MC 525 cells	NPMC 525 cells
Δ_0	0.1547	0.0108	0.0054	0.0012
Δ_1	2.47×10^{-15}	2.58×10^{-15}	1.57×10^{-16}	1.57×10^{-16}

Table 12
CPU time taken by numerical methods using constant coagulation kernel and linear selection function.

Method	Cells	Time taken (in seconds)	Cells	Time taken (in seconds)
MC	400	39.67	525	63.01
NPMC	400	38.92	525	60.17

4.2.2. Case (2): *additive coagulation kernel and constant selection function*

In order to check the accuracy and efficiency of the numerical methods, now the numerical results obtained using both approximations are compared with the newly derived exact moments. The exact results for the zeroth and first order moments are illustrated in Appendix A. The computational domain considered for comparison consists of particles ranging from $\vec{u}_{min} = 10^{-6}$ to $\vec{u}_{max} = 2 \times 10^4$ is divided into 20 cells along both directions for the case of two-dimensional PBE, that is, in total 20×20 cells are considered. The simulations are run until time $t = 2$. Similar to the previous case, the comparison of numerical and exact results predicted by approximating a two-dimensional PBE are shown in Fig. 10 for additive coagulation kernel and constant selection function. The plot shows that the zeroth order moment computed by the NPMC is matching well with the exact result, however, the MC shows slight deviation from the exact result. In addition, the first order moments are very well approximated by both methods, that is, the mass conservation property holds for both numerical methods. The quantitative errors in both moments are listed in Table 11 and it can be seen that the errors in moments obtained by NPMC are lesser as than the MC. Further, these errors can be reduced by increasing the number of cells in the given domain. Additionally, in terms of CPU time, Table 12 reveals that the NPMC is highly efficient than the MC, that is, the NPMC took lesser CPU time to compute the various results than the MC.

4.3. Simultaneous coagulation-fragmentation-3D

In order to enhance the comparison of numerical results with the exact results, we also compare the numerical results by approximating a 3D simultaneous coagulation-fragmentation equation in terms of integral moments. For the comparison, a additive coagulation kernel $\beta(u_1, u_2, u_1, u_1', u_2', u_3') = \beta_0(u_1 + u_2 + u_3 + u_1' + u_2' + u_3')$, constant selection function

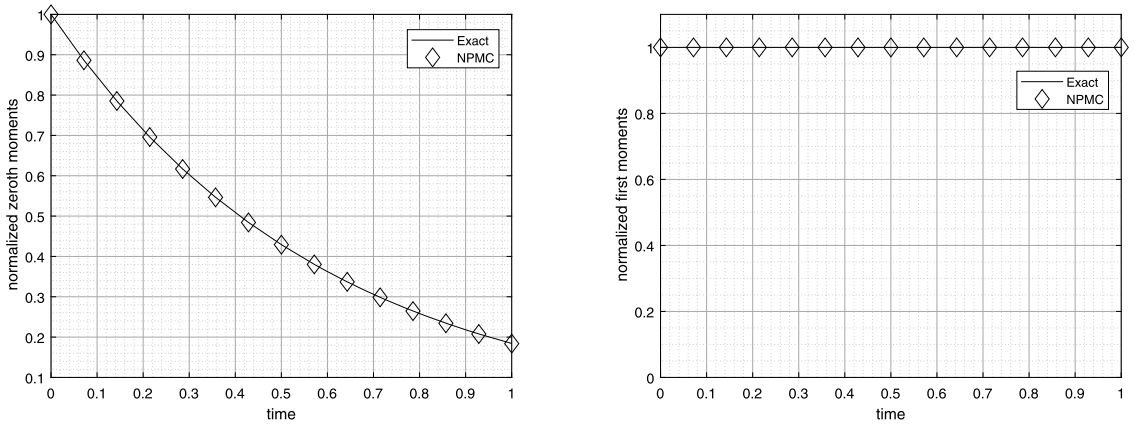

(a) Zeroth order moment ($\mu_{0,0,0}$) (b) First order moment ($\mu_{1,0,0} + \mu_{0,1,0} + \mu_{0,0,1}$)

Fig. 11. Comparison of various order moments for additive coagulation kernel and constant selection function.

($S(u_1, u_2, u_3) = S_0$) and binary breakage function ($b(u_1, u_2, u_3, u_1', u_2', u_3') = \frac{2}{u_1' u_2' u_3'}$) are considered. As we have seen from the 1D as well 2D cases that the NPMC method is emerged to be more accurate than the MC and existing cell average technique, hence only the comparison of NPMC is conducted against the analytical results. The computational domain taken for comparison consists of particles ranging from $\vec{u}_{min} = 10^{-6}$ to $\vec{u}_{max} = 5 \times 10^5$ is divided into $12 \times 12 \times 12$ non-uniform cells along three directions (u_1, u_2, u_3) for the case of a 3D simultaneous coagulation-fragmentation equation and the simulations are run until time $t = 1$. The analytical solutions for zeroth and first order moments corresponding to three dimensional simultaneous coagulation-fragmentation equation are provided in Appendix B. It can be seen from the Figs. 11(a) and 11(b) that the zeroth order moment predicted by the NPMC matches well with the analytical result even on a coarse grid. In addition, the first order moment also shows consistency, that is, the NPMC conserves the total mass in the system and matches well with the analytical result.

Finally, it can be concluded that the proposed methods are not only approximated a one-dimensional simultaneous coagulation-fragmentation PBE well but also can be easily extended to the higher dimensional simultaneous coagulation-fragmentation PBE. From the above discussion, it can be observed that discretization errors in the moments are not much enhanced and show very stable results when these finite volume schemes are extended to solve higher dimensional problems.

5. Conclusions

In the present work, two finite volume schemes for approximating a generalized simultaneous coagulation-fragmentation PBE on non-uniform grid are proposed. The qualitative and quantitative comparisons of the finite volume schemes with cell average technique in terms of different order moments have been shown for analytically tractable kernels. The results indicate that the NPMC predicts the various order moments as well as number density functions with equal or higher precision than the CAT with fewer grids, whereas the MC shows deviation for the zeroth order moment. However, both finite volume schemes are easy to code and consume lesser CPU than the CAT. Further, the errors in the different numerical results can be improved by considering a more refined grid and the MC method also achieved equal accuracy as both NPMC and CAT. Moreover, it has been also shown that the finite volume scheme can be easily extended to solve higher dimensional problems and are more stable numerical methods. We also derived the exact results for the moments corresponding to multidimensional PBE. Finally, it can be concluded that due to simpler mathematical formulations, the NPMC finite volume schemes are highly recommended for solving the problems related to the industrial applications involving twin screw granulation and sprayed fluidized bed granulation.

CRediT authorship contribution statement

Mehakpreet Singh: Conceptualization, Methodology, MATLAB Code, Writing – Original draft preparation, Investigation, Validation, Writing – Reviewing and Editing.

Declaration of competing interest

The authors declare that they have no known competing financial interests or personal relationships that could have appeared to influence the work reported in this paper.

Acknowledgement

The author gratefully acknowledges the financial support provided by Marie Skłodowska-Curie Individual Fellowship no. 841906 to Dr. Mehakpreet Singh.

Appendix A. Derivation of exact zeroth and first order moments-2D

For a vector $\vec{u} = (u_1, u_2)$, the two dimensional simultaneous coagulation-fragmentation PBE (38) can be rewritten as follows:

$$\begin{aligned}\frac{\partial n(t,u_1,u_2)}{\partial t} &= \frac{1}{2}\int_0^{u_1}\int_0^{u_2}\beta(t,u_1-u_1',u_2-u_2',u_1',u_2')n(t,u_1-u_1',u_2-u_2')n(t,u_1',u_2')\\ &\quad\times du_1'du_2' - \int_0^{\infty}\int_0^{\infty}\beta(t,u_1,u_2,u_1',u_2')n(t,u_1,u_2)n(t,u_1',u_2')du_1'du_2'\\ &\quad+\int_{u_1}^{\infty}\int_{u_2}^{\infty}b(u_1,u_2,u_1',u_2')S(u_1',u_2')n(t,u_1',u_2')du_1'du_2' - S(u_1,u_2)n(t,u_1,u_2),\end{aligned} \tag{A.1}$$

with initial data

$$n(0,u_1,u_2) = n_0(u_1,u_2)\,,\quad u_1,u_2\in]0,\infty[\,.$$

Multiplying the above equation by ${u_1}^r{u_2}^s$, integrating twice from 0 to ∞ and change the order of the first integral, we obtain the following equation in r,sth moment as

$$\begin{aligned}\frac{d\mu_{r,s}(t)}{dt} &= \int_0^{\infty}\int_0^{\infty}\int_0^{\infty}\int_0^{\infty}\Big[\frac{1}{2}(u_1+u_2+u_1'+u_2')^{rs} - (u_1+u_2)^r(u_1'+u_2')^s\Big]\beta(t,u_1,u_2,u_1',u_2')\\ &\quad\times n(t,u_1,u_2)n(t,u_1',u_2')du_1du_2du_1'du_2' + \int_0^{\infty}\int_0^{\infty}\Big[\int_0^{u_1'}\int_0^{u_2'}{u_1}^r{u_2}^s b(u_1,u_2,u_1',u_2')du_1du_2\\ &\quad-{u_1'}^r{u_2'}^s\Big]S(u_1',u_2')n(t,u_1',u_2')du_1'du_2'.\end{aligned} \tag{A.2}$$

Using $r=1,\ s=0$ and $r=0,\ s=1$, it is easy to show that $\frac{d\mu_{1,0}}{dt}=0$ and $\frac{d\mu_{0,1}}{dt}=0$. This is expected as the total mass in the system for the case of simultaneous coagulation-fragmentation PBE should be constant for any time. Next, our purpose is to derive the ordinary differential equation for the zeroth order moment, that is, $r=0,\ s=0$, as

$$\begin{aligned}\frac{d\mu_{0,0}(t)}{dt} &= -\frac{1}{2}\int_0^{\infty}\int_0^{\infty}\int_0^{\infty}\int_0^{\infty}\beta(t,u_1,u_2,u_1',u_2')n(t,u_1,u_2)n(t,u_1',u_2')du_1du_2du_1'du_2'\\ &\quad+\int_0^{\infty}\int_0^{\infty}\Big[\bar{N}(u_1',u_2')-1\Big]S(u_1',u_2')n(t,u_1',u_2')du_1'du_2'.\end{aligned} \tag{A.3}$$

Further simplification in the above equation can be done by assuming $\bar{N}(u_1',u_2') = p$ (constant) which is also used to calculate the exact solutions.

A.1. Case (1): *constant coagulation kernel and linear selection function*

Substituting the values of $\beta(u_1,u_2,u_1',u_2') = \beta_0(u_1+u_2+u_1'+u_2')$ and $S(u_1,u_2) = S_0(u_1+u_2)$ in equation (A.3), the following equation is obtained:

$$\frac{d\mu_{0,0}(t)}{dt} = -\frac{1}{2}\beta_0(\mu_{0,0})^2 + (p-1)S_0(\mu_{1,0}(0)+\mu_{0,1}(0)). \tag{A.4}$$

After simplification, we get the final expression for the zeroth order moment as

$$\mu_{0,0}(t) = c_1 \left[\frac{1 + c_2 \exp(\beta_0 c_1 t)}{1 - c_2 \exp(\beta_0 c_1 t)} \right], \tag{A.5}$$

where $c_1 = \sqrt{\frac{2(p-1)S_0(\mu_{1,0}(0) + \mu_{0,1}(0))}{\beta_0}}$ and $c_2 = \frac{\mu_{0,0}(0) - c_1}{\mu_{0,0}(0) + c_1}$.

A.2. Case (2): *additive coagulation kernel and constant selection function*

Substituting the values of $\beta(u_1, u_2, u_1', u_2') = \beta_0(u_1 + u_2 + u_1' + u_2')$ and $S(u_1, u_2) = S_0$ in equation (A.3), the following equation is obtained:

$$\frac{d\mu_{0,0}(t)}{dt} = -\frac{1}{2} 4\beta_0 \mu_{0,0}\mu_{1,0}(0) + (p-1)S_0\mu_{0,0}. \tag{A.6}$$

Solving the above equation will give us the following expression of the zeroth order moment

$$\mu_{0,0}(t) = c_1 \exp(-2\beta_0\mu_{1,0}(0)t + (p-1)S_0 t), \tag{A.7}$$

where $c_1 = \mu_{0,0}(0)$.

Appendix B. Derivation of exact zeroth and first order moments-3D

For a vector $\vec{u} = (u_1, u_2, u_3)$, the three dimensional simultaneous coagulation-fragmentation PBE (38) can be rewritten as follows:

$$\begin{aligned}
\frac{\partial n(t, u_1, u_2, u_3)}{\partial t} &= \frac{1}{2} \int_0^{u_1}\int_0^{u_2}\int_0^{u_3} \beta(t, u_1 - u_1', u_2 - u_2', u_3 - u_3', u_1', u_2', u_3') n(t, u_1 - u_1', u_2 - u_2', u_3 - u_3') \\
&\times n(t, u_1', u_2', u_3') du_1' du_2' du_3' - \int_0^{\infty}\int_0^{\infty}\int_0^{\infty} \beta(t, u_1, u_2, u_1', u_2', u_3') n(t, u_1, u_2, u_3) n(t, u_1', u_2', u_3') du_1' du_2' du_3' \\
&+ \int_{u_1}^{\infty}\int_{u_2}^{\infty}\int_{u_3}^{\infty} b(u_1, u_2, u_3, u_1', u_2', u_3') S(u_1', u_2', u_3') n(t, u_1', u_2', u_3') du_1' du_2' du_3' - S(u_1, u_2, u_3) n(t, u_1, u_2, u_3),
\end{aligned} \tag{B.1}$$

with initial data

$$n(0, u_1, u_2, u_3) = n_0(u_1, u_2, u_3), \quad u_1, u_2, u_3 \in]0, \infty[.$$

Multiplying equation (B.1) by ${u_1}^q {u_2}^r {u_3}^s$, integrating thrice from 0 to ∞ and change the order of the first integral, we obtain the following equation in q, r, sth moment as

$$\begin{aligned}
\frac{d\mu_{q,r,s}(t)}{dt} = &\int_0^{\infty}\int_0^{\infty}\int_0^{\infty}\int_0^{\infty}\int_0^{\infty}\int_0^{\infty} \Big[\frac{1}{2}(u_1 + u_2 + u_3 + u_1' + u_2' + u_3')^{qrs} - (u_1 + u_2)^q (u_1' + u_2')^r (u_3 + u_3')^s\Big] \\
&\beta(t, u_1, u_2, u_3, u_1', u_2', u_3') n(t, u_1, u_2, u_3) n(t, u_1', u_2', u_3') du_1 du_2 du_3 du_1' du_2' du_3' \\
&+ \int_0^{\infty}\int_0^{\infty}\int_0^{\infty} \Big[\int_0^{u_1'}\int_0^{u_2'}\int_0^{u_3'} {u_1}^q {u_2}^r {u_3}^s b(u_1, u_2, u_3, u_1', u_2', u_3') du_1 du_2 du_3 - {u_1'}^q {u_2'}^r {u_3'}^s \Big] \\
&\times S(u_1', u_2', u_3') n(t, u_1', u_2', u_3') du_1' du_2' du_3'.
\end{aligned} \tag{B.2}$$

Using $q = 1,\ r = 0,\ s = 0$; $q = 0,\ r = 1,\ s = 0$ and $q = 0,\ r = 0,\ s = 1$, it is easy to show that $\frac{d\mu_{1,0,0}}{dt} = 0$, $\frac{d\mu_{0,1,0}}{dt} = 0$ and $\frac{d\mu_{0,0,1}}{dt} = 0$ as the total mass in the system for a simultaneous coagulation-fragmentation PBE must be constant over the time domain. Next, let us derive the ordinary differential equation for the zeroth order moment, that is, for $q = 0,\ r = 0,\ s = 0$, the above equation can be written as

$$\frac{d\mu_{q,r,s}(t)}{dt} = \frac{-1}{2}\int_0^\infty\int_0^\infty\int_0^\infty\int_0^\infty\int_0^\infty\int_0^\infty \beta(t,u_1,u_2,u_3,u_1',u_2',u_3')n(t,u_1,u_2,u_3)n(t,u_1',u_2',u_3')$$
$$\times du_1du_2du_3du_1'du_2'du_3' + \int_0^\infty\int_0^\infty\int_0^\infty\left[\int_0^{u_1'}\int_0^{u_2'}\int_0^{u_3'} u_1^q u_2^r u_3^s b(u_1,u_2,u_1',u_2',u_3')du_1du_2du_3 - u_1'^q u_2'^r u_3'^s\right]$$
$$\times S(u_1',u_2')n(t,u_1',u_2',u_3')du_1'du_2'du_3'. \tag{B.3}$$

For simplification assume $\bar{N}(u_1',u_2',u_3') = p$ (constant) and further substituting the values of $S(u_1,u_2) = S_0$ and $\beta(u_1,u_2,u_3,u_1',u_2',u_3') = \beta_0(u_1+u_2+u_3+u_1'+u_2'+u_3')$ in equation (B.3), the following equation is obtained:

$$\frac{d\mu_{0,0,0}(t)}{dt} = -\frac{1}{2}6\beta_0\mu_{0,0,0}\mu_{1,0,0}(0) + (p-1)S_0\mu_{0,0,0}. \tag{B.4}$$

Solving the above equation will give us the following expression of the zeroth order moment

$$\mu_{0,0,0}(t) = c_1\exp(-3\beta_0\mu_{1,0,0}(0)t + (p-1)S_0t), \tag{B.5}$$

where $c_1 = \mu_{0,0,0}(0)$.

The generalized form of the zeroth order moment corresponding to simultaneous coagulation-fragmentation PBE having two or more internal coordinates is given by

$$\mu_{\lambda_1,\lambda_2,\cdots,\lambda_d}(t) = c_1\exp(-d\times\beta_0M_1(0)t + (p-1)S_0t). \tag{B.6}$$

Here $c_1 = \mu_{\lambda_1,\lambda_2,\cdots,\lambda_d}(0)$ where λ_k is zero for every k, $M_1(0)$ is the initial mass along the first internal coordinate and d represents the number of internal coordinates in the PBE.

References

[1] F. Ahamed, M. Singh, H.-S. Song, P. Doshi, C.W. Ooi, Y.K. Ho, On the use of sectional techniques for the solution of depolymerization population balances: results on a discrete-continuous mesh, Adv. Powder Technol. 31 (2020) 2669–2679.
[2] N. Ahmed, G. Matthies, L. Tobiska, Stabilized finite element discretization applied to an operator-splitting method of population balance equations, Appl. Numer. Math. 70 (2013) 58–79.
[3] M. Attarakih, M. Jaradat, C. Drumm, H. Bart, S. Tiwari, V. Sharma, J. Kuhnert, A. Klar, A multivariate sectional quadrature method of moments for the solution of the population balance equation, Comput.-Aided Chem. Eng. 28 (2010) 1551–1556.
[4] M.M. Attarakih, H.-J. Bart, N.M. Faqir, Solution of the droplet breakage equation for interacting liquid–liquid dispersions: a conservative discretization approach, Chem. Eng. Sci. 59 (12) (2004) 2547–2565.
[5] M.M. Attarakih, C. Drumm, H.J. Bart, Solution of the population balance equation using the sectional quadrature method of moments (SQMOM), Chem. Eng. Sci. 64 (4) (2009) 742–752.
[6] A. Braumann, M. Kraft, W. Wagner, Numerical study of a stochastic particle algorithm solving a multidimensional population balance model for high shear granulation, J. Comput. Phys. 229 (20) (2010) 7672–7691.
[7] A. Chaudhury, A. Kapadia, A.V. Prakash, D. Barrasso, R. Ramachandran, An extended cell-average technique for a multi-dimensional population balance of granulation describing aggregation and breakage, Adv. Powder Technol. 24 (6) (2013) 962–971.
[8] C. Dorao, H. Jakobsen, hp-adaptive least squares spectral element method for population balance equations, Appl. Numer. Math. 58 (5) (2008) 563–576.
[9] M. Ernst, R.M. Ziff, E. Hendriks, Coagulation processes with a phase transition, J. Colloid Interface Sci. 97 (1) (1984) 266–277.
[10] J.M. Fernández-Díaz, G.J. Gómez-García, Exact solution of a coagulation equation with a product kernel in the multicomponent case, Phys. D, Nonlinear Phenom. 239 (5) (2010) 279–290.
[11] F. Filbet, P. Laurençot, Numerical simulation of the Smoluchowski coagulation equation, SIAM J. Sci. Comput. 25 (6) (2004) 2004–2028.
[12] L. Forestier-Coste, S. Mancini, A finite volume preserving scheme on nonuniform meshes and for multidimensional coalescence, SIAM J. Sci. Comput. 34 (6) (2012) B840–B860.
[13] F. Guiaş, A stochastic approach for simulating spatially inhomogeneous coagulation dynamics in the gelation regime, Commun. Nonlinear Sci. Numer. Simul. 14 (1) (2009) 204–222.
[14] H.Y. Ismail, M. Singh, S. Darwish, M. Kuhs, S. Shirazian, D.M. Croker, M. Khraisheh, A.B. Albadarin, G.M. Walker, Developing ann-kriging hybrid model based on process parameters for prediction of mean residence time distribution in twin-screw wet granulation, Powder Technol. 343 (2019) 568–577.
[15] G. Kaur, M. Singh, T. Matsoukas, J. Kumar, T. De Beer, I. Nopens, Two-compartment modeling and dynamics of top-sprayed fluidized bed granulator, Appl. Math. Model. 68 (2019) 267–280.
[16] G. Kaur, R. Singh, M. Singh, J. Kumar, T. Matsoukas, Analytical approach for solving population balances: a homotopy perturbation method, J. Phys. A, Math. Theor. 52 (38) (2019) 385201.
[17] G. Kaur, R. Singh, M. Singh, J. Kumar, T. Matsoukas, Reply to comment on 'analytical approach for solving population balances: a homotopy perturbation method' (2019), J. Phys. A, Math. Theor. 52 (2020) 385201, J. Phys. A, Math. Gen. 53 (38), 388002.
[18] M. Kostoglou, Extended cell average technique for the solution of coagulation equation, J. Colloid Interface Sci. 306 (1) (2007) 72–81.
[19] M. Kostoglou, A. Karabelas, Evaluation of zero order methods for simulating particle coagulation, J. Colloid Interface Sci. 163 (2) (1994) 420–431.
[20] M. Kostoglou, A. Karabelas, On sectional techniques for the solution of the breakage equation, Comput. Chem. Eng. 33 (1) (2009) 112–121.
[21] A. Kumar, J. Vercruysse, V. Vanhoorne, M. Toiviainen, P.-E. Panouillot, M. Juuti, C. Vervaet, J.P. Remon, K.V. Gernaey, T. De Beer, et al., Conceptual framework for model-based analysis of residence time distribution in twin-screw granulation, Eur. J. Pharm. Sci. 71 (2015) 25–34.
[22] J. Kumar, G. Kaur, E. Tsotsas, An accurate and efficient discrete formulation of aggregation population balance equation, Kinet. Relat. Models 9 (2) (2016) 373–391.
[23] J. Kumar, M. Peglow, G. Warnecke, S. Heinrich, L. Mörl, Improved accuracy and convergence of discretized population balance for aggregation: the cell average technique, Chem. Eng. Sci. 61 (10) (2006) 3327–3342.

[24] J. Kumar, G. Warnecke, M. Peglow, S. Heinrich, Comparison of numerical methods for solving population balance equations incorporating aggregation and breakage, Powder Technol. 189 (2) (2009) 218–229.
[25] R. Kumar, J. Kumar, G. Warnecke, Moment preserving finite volume schemes for solving population balance equations incorporating aggregation, breakage, growth and source terms, Math. Models Methods Appl. Sci. 23 (07) (2013) 1235–1273.
[26] S. Kumar, D. Ramkrishna, On the solution of population balance equations by discretization–I. A fixed pivot technique, Chem. Eng. Sci. 51 (8) (1996) 1311–1332.
[27] S. Le Borne, L. Shahmuradyan, Algorithms for the Haar wavelet based fast evaluation of aggregation integrals in population balance equations, Appl. Numer. Math. 108 (2016) 1–20.
[28] Y. Liao, R. Oertel, S. Kriebitzsch, F. Schlegel, D. Lucas, A discrete population balance equation for binary breakage, Int. J. Numer. Methods Fluids 87 (4) (2018) 202–215.
[29] F. Lin, S.V. Meleshko, A.E. Flood, Exact solutions of the population balance equation including particle transport, using group analysis, Commun. Nonlinear Sci. Numer. Simul. 59 (2018) 255–271.
[30] Y. Lin, K. Lee, T. Matsoukas, Solution of the population balance equation using constant-number Monte Carlo, Chem. Eng. Sci. 57 (12) (2002) 2241–2252.
[31] D.L. Marchisio, R.O. Fox, Solution of population balance equations using the direct quadrature method of moments, J. Aerosol Sci. 36 (1) (2005) 43–73.
[32] D. Patil, J. Andrews, An analytical solution to continuous population balance model describing floc coalescence and breakage–a special case, Chem. Eng. Sci. 53 (3) (1998) 599–601.
[33] R.I. Patterson, W. Wagner, M. Kraft, Stochastic weighted particle methods for population balance equations, J. Comput. Phys. 230 (19) (2011) 7456–7472.
[34] M. Pigou, J. Morchain, P. Fede, M.-I. Penet, G. Laronze, New developments of the extended quadrature method of moments to solve population balance equations, J. Comput. Phys. 365 (2018) 243–268.
[35] S. Qamar, I. Angelov, M. Elsner, A. Ashfaq, A. Seidel-Morgenstern, G. Warnecke, Numerical approximations of a population balance model for coupled batch preferential crystallizers, Appl. Numer. Math. 59 (3–4) (2009) 739–753.
[36] S. Qamar, G. Warnecke, Numerical solution of population balance equations for nucleation, growth and aggregation processes, Comput. Chem. Eng. 31 (12) (2007) 1576–1589.
[37] S. Qamar, G. Warnecke, Solving population balance equations for two-component aggregation by a finite volume scheme, Chem. Eng. Sci. 62 (3) (2007) 679–693.
[38] A. Ranodolph, Theory of Particulate Processes: Analysis and Techniques of Continuous Crystallization, Elsevier, 2012.
[39] J. Saha, J. Kumar, A. Bück, E. Tsotsas, Finite volume approximations of breakage population balance equation, Chem. Eng. Res. Des. 110 (2016) 114–122.
[40] S. Shirazian, H.Y. Ismail, M. Singh, R. Shaikh, D.M. Croker, G.M. Walker, Multi-dimensional population balance modelling of pharmaceutical formulations for continuous twin-screw wet granulation: determination of liquid distribution, Int. J. Pharm. 566 (2019) 352–360.
[41] M. Singh, J. Chakraborty, J. Kumar, R. Ramakanth, Accurate and efficient solution of bivariate population balance equations using unstructured grids, Chem. Eng. Sci. 93 (2013) 1–10.
[42] M. Singh, D. Ghosh, J. Kumar, A comparative study of different discretizations for solving bivariate aggregation population balance equation, Appl. Math. Comput. 234 (2014) 434–451.
[43] M. Singh, H.Y. Ismail, T. Matsoukas, A.B. Albadarin, G. Walker, Mass-based finite volume scheme for aggregation, growth and nucleation population balance equation, Proc. R. Soc. A 475 (2231) (2019) 20190552.
[44] M. Singh, H.Y. Ismail, R. Singh, A.B. Albadarin, G. Walker, Finite volume approximation of nonlinear agglomeration population balance equation on triangular grid, J. Aerosol Sci. 137 (2019) 105430.
[45] M. Singh, G. Kaur, Convergence analysis of finite volume scheme for nonlinear aggregation population balance equation, Math. Methods Appl. Sci. 42 (9) (2019) 3236–3254.
[46] M. Singh, G. Kaur, T. De Beer, I. Nopens, Solution of bivariate aggregation population balance equation: a comparative study, React. Kinet., Mech. Catal. 123 (2018) 385–401.
[47] M. Singh, G. Kaur, J. Kumar, T. De Beer, I. Nopens, A comparative study of numerical approximations for solving the Smoluchowski coagulation equation, Braz. J. Chem. Eng. 35 (4) (2018) 1343–1354.
[48] M. Singh, A. Kumar, S. Shirazian, V. Ranade, G. Walker, Characterization of simultaneous evolution of size and composition distributions using generalized aggregation population balance equation, Pharmaceutics 12 (12) (2020) 1152.
[49] M. Singh, J. Kumar, A. Bück, E. Tsotsas, A volume-consistent discrete formulation of aggregation population balance equations, Math. Methods Appl. Sci. 39 (9) (2015) 2275–2286.
[50] M. Singh, J. Kumar, A. Bück, E. Tsotsas, An improved and efficient finite volume scheme for bivariate aggregation population balance equation, J. Comput. Appl. Math. 308 (2016) 83–97.
[51] M. Singh, T. Matsoukas, A.B. Albadarin, G. Walker, New volume consistent approximation for binary breakage population balance equation and its convergence analysis, ESAIM: Math. Model. Numer. Anal. 53 (5) (2019) 1695–1713.
[52] M. Singh, T. Matsoukas, G. Walker, Mathematical analysis of finite volume preserving scheme for nonlinear Smoluchowski equation, Phys. D, Nonlinear Phenom. 402 (2020) 132221.
[53] M. Singh, R. Singh, S. Singh, G. Singh, G. Walker, Finite volume approximation of multidimensional aggregation population balance equation on triangular grid, Math. Comput. Simul. 172 (2020) 191–212.
[54] M. Singh, R. Singh, S. Singh, G. Walker, T. Matsoukas, Discrete finite volume approach for multidimensional agglomeration population balance equation on unstructured grid, Powder Technol. 376 (2020) 229–240.
[55] M. Singh, K. Vuik, G. Kaur, H.-J. Bart, Effect of different discretizations on the numerical solution of 2D aggregation population balance equation, Powder Technol. 342 (2019) 972–984.
[56] M. Smith, T. Matsoukas, Constant-number Monte Carlo simulation of population balances, Chem. Eng. Sci. 53 (9) (1998) 1777–1786.
[57] M. Vanni, Approximate population balance equations for aggregation–breakage processes, J. Colloid Interface Sci. 221 (2) (2000) 143–160.